NTNU

Application of nek5000 to dispersion simulations

Author:
Magnus Aarskaug Rud

Supervisor:
Anne Kværnø

Research Group Name

IMF

January 2016

NTNU

Abstract

Faculty Name

IMF

Master Thesis

Application of nek5000 to dispersion simulations

by Magnus Aarskaug Rud

Sed ullamcorper quam eu nisl interdum at interdum enim egestas. Aliquam placerat justo sed lectus lobortis ut porta nisl porttitor. Vestibulum mi dolor, lacinia molestie gravida at, tempus vitae ligula. Donec eget quam sapien, in viverra eros. Donec pellentesque justo a massa fringilla non vestibulum metus vestibulum. Vestibulum in orci quis felis tempor lacinia. Vivamus ornare ultrices facilisis. Ut hendrerit volutpat vulputate. Morbi condimentum venenatis augue, id porta ipsum vulputate in. Curabitur luctus tempus justo. Vestibulum risus lectus, adipiscing nec condimentum quis, condimentum nec nisl.

CONTENTS

NOTATION

CONVENTION	we let subscript h denote the discretized variables
u	the velocity field
p	pressure
f	source function / loading function
ν	kinematic viscosity
U	Freestream velocity / velocity scale
L	Length scale
$Re = UL/\nu$	Reynolds number
d	The dimension of the problem, in this thesis $d = 3$
Ω	Some general domain in $\mathbb{R}^d$
$s_{ij} = 1/2(\nabla \mathbf{u} + \nabla^T \mathbf{u})$	Strain-rate tensor
$\mathcal{S} = |s_{ij}| = \sqrt{2s_{ij}s_{ij}}$	Absolute value of the strain-rate tensor
τ_{ij}	subgrid-scale tensor
$\mathcal{A}$	The bilinear Laplace operator
$\mathcal{B}$	The bilinear divergence operators
$\mathcal{C}$	The trilinear convection operators
A	The stiffness matrix
D	The divergence matrix
C	The convection matrix
M	The mass matrix
H	The Helmholtz matrix
$||u||$	the L^2 norm of u
$||u||_m$	the H^m norm of u
$||u||_{m,k}$	the H^m norm of u on the domain Ω_k

CHAPTER 1

INTRODUCTION

The physics regarding fluids in motion are described mathematically by the Navier-Stokes (N-S) equations. They are a result of the conservation of momentum and mass, and it is referred to [1] for a complete description of the necessary assumptions and simplifications. This thesis is restricted to numerical solutions of the incompressible N-S equations. Without further introduction the incompressible N-S equations are stated as

$$\frac{\partial \mathbf{u}}{\partial t} + \mathbf{u} \cdot \nabla \mathbf{u} = -\nabla p + \frac{1}{Re}\Delta \mathbf{u} + \mathbf{f},$$

$$\nabla \cdot \mathbf{u} = 0. \tag{1.1}$$

$\mathbf{u}$ and p denotes the velocity of the fluid and the pressure, while $\mathbf{f}$ is some external force. The Reynolds number Re describes the relation between the viscous scales and the mean stream velocity scale. For large Reynolds numbers the flow becomes turbulent and a large range of scales needs to be resolved. A lot of research has been devoted to determine the amount of energy present at the different scales of motion, and the interaction between them. This approach to Eq. (2.1) leads to turbulence modelling which is based on the idea that the effect of the smallest turbulent motions can be modelled while the larger motions are resolved by the numerical grid. In this thesis both laminar and turbulent flows will be solved numerically, and a turbulence model will also be compared to a mathematical filter meant to stabilize the flow. In addition to solving the N-S equations the transport of a passive scalar will also be analysed and compared to a set of reference solutions. The software applied in this thesis is Nek5000 which is an implementation of the spectral element method initialized in the 80's. In

addition to validate Nek5000 as a software for analyzing gas dispersion it is also as a part of this thesis attempted to make Nek5000 more applicable to cases consisting of more complex geometry.

The thesis is divided in 3 parts. The first part which includes the two following chapters are devoted to the physical understanding of Eq. (2.1), the solution methods and a thorough presentation of the spectral element method. Chapter 4 gives the reader a brief introduction to the functionalities of the solver Nek5000 to motivate some of the implementation performed. The last two chapters describes the work performed by the author, first a presentation of the different cases followed by the results and the discussion of these.

CHAPTER 2

PROBLEM DESCRIPTION

This chapter will present the Incompressible Navier-Stokes equations and give a thorough analysis of the physical effects of each term. It will also present the idea behind turbulence modelling, and prepare the mathematical formulations that will be further analysed in Chapter 3.

2.1 THE INCOMPRESSIBLE NAVIER-STOKES EQUATIONS

With the assumption of an incompressible flow the conservation of mass results in a divergence free restriction on the velocity $\mathbf{u}$ and the incompressible N-S equations on a domain $\Omega \subset \mathbb{R}^d$ can be stated as

$$\frac{\partial \mathbf{u}}{\partial t} + \mathbf{u} \cdot \nabla \mathbf{u} = -\nabla p + \frac{1}{Re}\Delta \mathbf{u} + \mathbf{f}, \qquad \nabla \cdot \mathbf{u} = 0, \qquad \text{on } \Omega. \tag{2.1}$$

A commonly studied simplification of this problem is the Stokes problem which is obtained by omitting the convective term. This thesis will use the Stokes problem as a starting point for analysis of the full problem in Chapter 3.1. Before attempting to solve these equations it is important to understand the role of each term and their mathematical influence on the problem.

- $\partial \mathbf{u}/\partial t$ - The time-derivative of the flow, for a steady state flow this term will be equal zero. The discretization of this term is often based on some implicit scheme.

- $\mathbf{u} \cdot \nabla \mathbf{u}$ - The convective term, describes the transport due to the flow itself on each of its components. The term is not present in Stokes problem. The mathematical operator corresponding to this term is non-linear and non-symmetric, and does therefore require an explicit scheme. Even with linear advection the operator quickly leads to instability.

- ∇p - The pressure gradient, removal of this term results in a pure advection diffusion problem.

- Re - The Reynolds number defined as UL/ν where U is the velocity scale, L is the length scale and ν is the viscosity of the fluid. Re describes the relation between the largest length scales of the flow and the viscous length scales. Notice that for large Reynolds numbers the unstable non-linear term dominates the transportation. Turbulent flows are characterized by a high Reynolds number.

- $\Delta \mathbf{u}$ - The diffusive term describes the natural diffusion of the fluid. The contribution of the diffusional term is inversely proportional to the Reynolds number. The corresponding mathematical operator stabilizes the system and it is therefore generally easier to solve the N-S equations for high-viscosity fluids. It should be mentioned that this term is actually a simplification of the Reynolds stress tensor that can be made under the assumption of incompressibility. The more general formulation that will be used in Chapter 2.3 is $2\nabla s_{ij}$, the tensor s_{ij} is known as the strain-rate tensor.

- $\mathbf{f}$ - General term describing external body forces such as gravity. For incompressible flow the gravity term is incorporated in the pressure term, $\nabla p = \nabla p + \rho \mathbf{g}$.

- $\nabla \cdot \mathbf{u}$ - The divergence free condition appears naturally from the conservation of mass in an incompressible flow.

For large Reynolds numbers the huge span in length scales requires a very fine mesh if Eq. (2.1) are to be solved exactly. Because a fine mesh implies a high computational cost a direct numerical solution (DNS) is not feasible for problems of a certain geometrical complexity. There are many different approaches on how to resolve the turbulent term and in this thesis the main approach will be through Large Eddy Simulations (LES) which will be discussed in Chapter 2.3. The Navier-Stokes equations can only be solved if the boundary conditions are given. The boundary conditions are not stated explicitly

in Eq. (2.1) because they depend on the physical situation and belong as a specification to each individual case. The next subsection gives a quick overview of the different boundary conditions applied in this thesis.

2.1.1 BOUNDARY CONDITIONS

Depending on the kind of flow and geometry a particular problem different boundary conditions are applied. In this section $\mathbf{n}$ and $\mathbf{t}$ will denote the normal and tangent vector to the surface. The boundary conditions applied for the cases investigated in this thesis will be given the names I,O,SYM and W for Inflow, Outflow, Symmetry and Wall. Their mathematical formulation and physical interpretation are given as

- I - Inflow, defining the velocity field on the boundary. Mathematically this is equivalent to non-homogeneous Dirichlet conditions.

$$\mathbf{u} = \mathbf{g}(\mathbf{x}, t). \tag{2.2}$$

- O - Outflow, letting the fluid flow "effortlessly" out through the boundary. Formally stated as

$$\frac{1}{Re}\nabla\mathbf{u} \cdot \mathbf{n} - p\mathbf{n} = 0. \tag{2.3}$$

- SYM - Symmetry, denying any flux through the boundary without disturbing the tangential velocity. Convenient to apply in an open channel where the stream wise direction is parallel to the boundary. Mathematically this is described as

$$\mathbf{u} \cdot \mathbf{n} = 0, \qquad (\nabla\mathbf{u} \cdot \mathbf{t}) \cdot \mathbf{n} = 0. \tag{2.4}$$

- W - Wall, Representing a physical object. Also known as the no-slip condition which is based on the assumption that the fluid closest to the object moves with the same speed as the object itself. In this thesis all objects and geometries is kept still so mathematically this is equivalent to homogeneous Dirichlet conditions.

$$\mathbf{u} = 0. \tag{2.5}$$

<center>2.1.2   WEAK FORMULATION OF N-S</center>

The numerical algorithms applied in this thesis requires a weak formulation of Eq. (2.1). Before the weak form is derived a few operators will be defined in order to simplify the final expression.

$$(\mathbf{u}, \mathbf{v}) = \int_{\Omega} \mathbf{u} \cdot \mathbf{v} d\Omega \tag{2.6}$$

$$\mathcal{A}(\mathbf{u}, \mathbf{v}) = \nu(\nabla \mathbf{u}, \nabla \mathbf{v}) \tag{2.7}$$

$$\mathcal{B}(\mathbf{u}, p) = -(\nabla \cdot \mathbf{u}, p) \tag{2.8}$$

$$\mathcal{C}(\mathbf{w}; \mathbf{u}, \mathbf{v}) = (\mathbf{w} \cdot \nabla \mathbf{u}, \mathbf{v}) \tag{2.9}$$

A weak formulation is obtained by multiplying with a test function $\mathbf{v}$ and integrating over the entire domain.

$$\int_{\Omega} \frac{\partial \mathbf{u}}{\partial t} \cdot \mathbf{v} d\Omega + \int_{\Omega} (\mathbf{u} \cdot \nabla) \mathbf{u} \cdot \mathbf{v} d\Omega = -\int_{\Omega} \nabla p \cdot \mathbf{v} d\Omega + \nu \int_{\Omega} \Delta \mathbf{u} \cdot \mathbf{v} d\Omega + \int_{\Omega} \mathbf{f}, \mathbf{v} d\Omega$$
$$\int_{\Omega} (\nabla \cdot \mathbf{u}) q d\Omega = 0. \tag{2.10}$$

Introducing the compact inner product notation and applying the divergence theorem on the right hand side of the first equation yields

$$(\frac{\partial \mathbf{u}}{\partial t}, \mathbf{v}) + (\mathbf{u} \cdot \nabla \mathbf{u}, \mathbf{v}) = (\nabla \cdot \mathbf{v}, p) - \nu(\nabla \mathbf{u}, \nabla \mathbf{v}) + (\mathbf{f}, \mathbf{v})$$
$$(\nabla \cdot \mathbf{u}, q) = 0. \tag{2.11}$$

The contributions from the boundary as a result from the application of the divergence theorem is included in the force term. The choice of search spaces for the velocity and pressure will be justified in Chapter 3, and will just be stated here in order to present the weak formulation. Let $V \subset H^1(\Omega)^3$ and $Q \subset L^2(\Omega)$ be subspaces that include the boundary conditions given by any particular flow situation. By using the notation introduced in Eq. (2.9) the weak formulation of the incompressible N-S equations can be stated as:

Find $(\mathbf{u}, p) \in V \times Q$ such that

$$(\frac{\partial \mathbf{u}}{\partial t}, \mathbf{v}) + \mathcal{C}(\mathbf{u}; \mathbf{u}, \mathbf{v}) = -\mathcal{B}(\mathbf{v}, p) - \mathcal{A}(\mathbf{u}, \mathbf{v}) + (\mathbf{f}, \mathbf{v}),$$
$$\mathcal{B}(\mathbf{u}, q) = 0, \tag{2.12}$$

$\forall\, (\mathbf{v}, q) \in V \times Q.$

In order to solve this equation numerically, everything has to be discretized and expressed using a set of basis functions. The idea is that the solution $(\mathbf{u}, p)$ is approximated by a discretized solution $(\mathbf{u}_h, p_h)$ and the bilinear operators can be represented by matrices. The discretized system of equations can be stated as

$$M\frac{\partial \mathbf{u}_h}{\partial t} + C(\mathbf{u}_h)\mathbf{u}_h = D^T p_h - \nu A \mathbf{u}_h + M\mathbf{f}_h, \qquad (2.13)$$

$$D\mathbf{u}_h = 0. \qquad (2.14)$$

2.2 The passive scalar equation

The N-S equations explains how a fluid will behave and solving it provides a complete pressure-velocity field of the domain of interest, but it does not provide the answer of how a scalar such as heat or a neutral gas will move in this flow. The equation corresponding to the motion of a scalar ϕ in a velocity field $\mathbf{u}$ will be referred to as the passive scalar (PS) equation and is stated as

$$\rho c_p \left(\frac{\partial \phi}{\partial t} + \mathbf{u} \cdot \nabla \phi \right) = \nabla \cdot (k \nabla \phi) + q_{vol}. \qquad (2.15)$$

The constants k and ρc_p are interpreted depending on the scalar transported. For dispersion of neutral gas with ϕ as the volume concentration of the gas they resemble the viscosity and mass flux. The last term on the right hand side q_{vol} is the source term and is not included in this thesis since all gas enters the control volume as a boundary condition.

The passive scalar equation is solved as a Helmholtz problem, by applying a explicit scheme on the convection term and an implicit scheme on the diffusion term. This is similar to the discretization performed on the momentum equation which will be discussed in detail in Chapter 3.

2.3 RESOLVING THE TURBULENT TERM USING LES

When DNS is not feasible due to high Reynolds number on large domains LES is one of the most powerful tools for simulating turbulent flows. The idea is based on the fact that the small turbulent structures behave homogeneously and are therefore easy to model. This way the larger structures driven by geometry, inflow conditions and external forces can be simulated using a coarser grid while the effect of the small structures are modelled. LES will be introduced here in a mathematical fashion, although in many practical cases the filter function is not well defined. The reason for this is that the grid itself is often considered a filter, with the grid size as the filter width. As pointed out by Carati et al. [2] the filter is in this case nothing else but numerical discretization error.

2.3.1 FILTER

The idea behind LES starts with defining a filter, which separates the modelled structures from the resolved ones. A filter in its general mathematical form introduced by Leonard [3] is given as

$$U^r(\mathbf{x}, t) = \int_\Omega G_r(\mathbf{r}, \mathbf{x}) U(\mathbf{x} - \mathbf{r}, t) d\mathbf{r} \qquad (2.16)$$

It is generally assumed that the filter commutes with the differential operators ∇, Δ and $\partial/\partial t$. By applying the filter on the N-S equations and making the given assumptions the filtered N-S equations can be stated as

$$\frac{\partial \mathbf{u}^r}{\partial t} + \mathbf{u}^r \cdot \nabla \mathbf{u}^r = -\nabla p^r + \nu \Delta \mathbf{u}^r + \mathbf{f}^r - \nabla \cdot \tau,$$
$$\nabla \cdot \mathbf{u}^r = 0. \qquad (2.17)$$

Where τ in this case denotes the subgrid-scale (SGS) stress given as

$$\tau_{ij}(u_i, uj) = (u_i u_j)^r - u_i^r u_j^r. \qquad (2.18)$$

This tensor is a consequence of applying the filter on the non-linear advection term, and it is this tensor that is modelled by a subgrid-scale model. See [4] for a full derivation on the application of a filter on the momentum equation.

2.3.2 Dynamic Smagorinsky-Lilly SGS-model

The problem is now reduced to modelling the tensor τ_{ij}, one of the most common SGS-models is the dynamic Smagorinsky-Lilly model which is the one applied in this thesis. The initial progress of this model was made by Lilly in 1967 [5] suggesting the following model for the SGS-tensor

$$
\begin{aligned}
\tau_{ij} &= -2C_s l^2 \mathcal{S}^r s_{ij}^r, \\
s_{ij}^r &= \frac{1}{2}\left(\frac{\partial u_i^r}{\partial x_j} + \frac{\partial u_j^r}{\partial x_i}\right), \\
\mathcal{S}^r &= \sqrt{2 s_{ij}^r s_{ij}^r}.
\end{aligned}
\tag{2.19}
$$

Where l denotes the filter width, which for this thesis is equivalent to the grid size. The resolved strain rate s_{ij}^r can be calculated from the filtered velocity and the problem is now reduced to determining the constant C_s. There were several attempts to determine this constant for the entire domain, but in lack of a general constant applicable to all flow situations a dynamic constant C_d was presented to replaces $C_s l^2$ in Eq. (2.19). C_d is called the dynamic Smagorinsky constant, and is both time and space dependent. The general idea is that C_d is unaffected by the filter and from this assumption an computable expression is developed for the dynamical constant.

Let a, b denote two distinct filters with corresponding filter widths l_a, l_b. Throughout this thesis l_a will be the grid size and $l_b \approx 2l_a$. Filter b is often referred to as the test filter and is only included to provide an estimation of the dynamic Smagorinsky constant. Remember that l_a is the grid size while filter b is obtained by applying the filter described in Chapter 3.4.2 with $\alpha_i = 1$ for the highest modes. Let τ_{ij} and T_{ij} denote the stresses based on single- and double filtering operations on the N-S equations

$$
\begin{aligned}
\tau_{ij} &= (u_i u_j)^a - u_i^a u_j^a, \\
T_{ij} &= ((u_i u_j)^a)^b - (u_i^a)^b (u_j^a)^b.
\end{aligned}
\tag{2.20}
$$

Applying the b filter on the first tensor in Eq. (2.20) allows us to define a new tensor L_{ij} that depends only on the a-filtered variables. The identity is known as the Germano identity and was first introduced in 1991 [6],

$$
L_{ij} = T_{ij} - (\tau_{ij})^b = (u_i^a u_j^a)^b - (u_i^a)^b (u_j^a)^b.
\tag{2.21}
$$

This tensor now depends on the a-filtered solution and not the resolved one, hence the identity in Eq. (2.21) provides a computable expression for L_{ij}.

Substituting the stress-tensors with their corresponding expression from Eq. (2.19) and assuming a dynamic constant unaffected by the filter one obtains an approximation for L_{ij} which is also computable,

$$
\begin{aligned}
L_{ij} &\approx 2C_s l_b^2 \mathcal{S}^{ab} s_{ij}^{ab} - 2(C_s l_a^2 \mathcal{S}^a s_{ij}^a)^b \\
&\approx 2C_s l_a^2 [\lambda^2 \mathcal{S}^{ab} s_{ij}^{ab} - (\mathcal{S}^a s_{ij}^a)^b] \\
&= 2C_d M_{ij}.
\end{aligned}
\tag{2.22}
$$

$$
M_{ij} = \lambda^2 \mathcal{S}^{ab} s_{ij}^{ab} - (\mathcal{S}^a s_{ij}^a)^b
\tag{2.23}
$$

$$
C_d = C_s l_a^2
\tag{2.24}
$$

$$
\lambda = l_b / l_a
\tag{2.25}
$$

Minimizing the mean-square error between the exact L_{ij} as expressed in Eq. (2.21) and the Boussinesq-based approximation in Eq. (2.22) yields the best approximation for the dynamic Smagorinsky constant

$$
C_s = \frac{M_{ij} L_{ij}}{2 M_{kl} M_{kl}}.
\tag{2.26}
$$

Note that the double indices implies summing. This expression is however not a stable option and to deal with this most implementations apply some sort of mean or smoothening in either time and/or space when calculating the constant. In this thesis the smoothening is done in both time and space for the denominator and the numerator in Eq. (2.26). Another property of this expression is that the constant C_d is independent of the filter width, the only necessary variable is the coefficient $\lambda = l_b / l_a$. The assumption made in this model is that turbulence behaves as diffusion, similar to the kinematic viscosity a turbulent viscosity ν_t is defined which for this case is given as $\nu_t = C_s \mathcal{S}^a$.

Let us end this section by stating the filtered N-S equations with the LES using dynamical Smagorinsky subgrid scale model, and remember that the diffusive term is written

in general terms as $2\nabla \cdot \nu s_{ij}$.

$$\frac{\partial \mathbf{u}^a}{\partial t} + \mathbf{u}^a \cdot \nabla \mathbf{u}^a = -\nabla p^a + \mathbf{f}^a + 2\nabla \cdot (\nu + \nu_t) s_{ij}^a$$

$$\nabla \cdot \mathbf{u}^a = 0. \tag{2.27}$$

Notice that if v_t is a constant in the entire domain this equation would be equivalent to the one for a fluid with viscosity $\nu' = \nu + \nu_t$. The idea is that ν_t will be larger when the subgrid-structures are significant and closer to zero when the flow is laminar. This is just one of many types of models but is attractive due to its simple derivation from physical principles.

CHAPTER 3

NUMERICAL ALGORITHMS

3.1 NUMERICAL CONCEPTS ON THE STOKES PROBLEM

In the previous chapter the N-S equations were presented and reformulated in several ways without any details on how to actually solve the equations. This chapter aims to give a more detailed description of the solution methods applied. The choice of algorithms and solution spaces requires a more thorough analysis which is normally performed on the steady Stokes problem. The steady Stokes problem does not include the convection term or the time derivative but the highest order terms are all present and is therefore a valid problem to perform this necessary analysis [7]. The time schemes applied will be discussed in Chapter 3.5. The steady Stokes problem with homogeneous boundary conditions is given as

$$-\mu\Delta\mathbf{u} + \nabla p = \mathbf{f}, \qquad \nabla\cdot\mathbf{u} = 0,$$
$$\mathbf{u} = \mathbf{0} \text{ on } \partial\Omega. \tag{3.1}$$

Applying the weak formulation to the Stokes problem implies a minimum requirement on the spaces for $\mathbf{u}$ and p, and their test functions. These spaces will be defined as

$$H_0^1(\Omega)^3 = \left\{\mathbf{v} \in H^1(\Omega)^3 \mid \mathbf{v} = \mathbf{0} \text{ on } \partial\Omega\right\},$$
$$L_0^2(\Omega) = \left\{q \in L^2(\Omega) \mid \int_\Omega q dx = 0\right\}, \tag{3.2}$$

The formulation can easily be extended to include inhomogeneous Dirichlet conditions on $\mathbf{u}$ by defining a lifting function as described in [8]. Note also that the pressure is

only present through its gradient and is therefore not uniquely defined unless the extra constraint on the mean is defined, hence the 0 in L_0^2. The weak form can now be stated as

Find $(\mathbf{u}, p) \in H_0^1(\Omega)^3 \times L_0^2(\Omega)$ such that

$$\mathcal{B}(\mathbf{v}, p) + \mathcal{A}(\mathbf{u}, \mathbf{v}) = (\mathbf{f}, \mathbf{v}),$$
$$\mathcal{B}(\mathbf{u}, q) = 0. \tag{3.3}$$

$\forall\, (\mathbf{v}, q) \in H^1(\Omega)^3 \times L^2(\Omega)$.

The numerical solution of this problem requires a discrete formulation of the weak form, with $(\mathbf{u}_h, p_h) \in V \times Q$ as the discrete solution. The discrete spaces V, Q are subspaces of $H_0^1(\Omega)^3, L_0^2(\Omega)$ equipped with the discrete $H^1(\Omega)^3$- and $L^2(\Omega)$-norm denoted $||\cdot||_V$ and $||\cdot||_Q$. For the discrete weak form to be well-posed it has to meet the requirements stated by the inf-sup condition. This condition is known from the study of saddle-point problems, and is often referred to as the Babuska-Brezzi condition due to their important results in [9] and [10]. The name inf-sup is a result of the following way of writing it,

$$\inf_{q \in Q} \sup_{\mathbf{v} \in V} \frac{\mathcal{B}(v, q)}{||\mathbf{v}||_V ||q||_Q} \geq b. \tag{3.4}$$

Where b denotes some positive constant. Fulfilling this condition often implies a staggered grid, such that the pressure and the velocity are evaluated at different points. For a Spectral Element formulation of this problem which will be elaborated in Chapter 3.4, a valid choice of subspaces (V, Q) is $\left(\left[P_N \cap H_0^1\right]^3, P_{N-2} \cap L_0^2\right)$. This will be referred to as the $P_N P_{N-2}$-formulation where P_N denotes the space of polynomials up to degree N. It was however proved by Guermond in [11] that the fractional step algorithm applies a form of the Stokes problem which automatically fulfills the inf-sup condition and therefore does not require any particular discrete subspaces to be chosen. For the sake of convenience the polynomial degree of the pressure and the velocity will be the same and the discrete pair of subspaces (V, Q) is chosen to $\left(\left[P_N \cap H_0^1\right]^3, P_N \cap L_0^2\right)$, known as the $P_N P_N$-formulation.

Before the analysis of the N-S equations can be taken any further the theory behind the Spectral Element Method will be presented in the following subsections.

3.2   FINITE ELEMENT METHOD

Finite element method (FEM) is one of the most widely used numerical methods applied on problems within construction, flow simulation and many other areas. It offers a precise mathematical foundation and due to the connectivity properties of the elements it guaranties a sparse system. The decomposition of the geometrical domain into a finite amount of elements, makes it possible to create general algorithms applicable to all kinds of geometries. For the full mathematical foundation of FEM it will be referred to [8], but some of the key properties will be stated here in order to provide a thorough understanding of the spectral element method (SEM). Throughout this section p denotes the polynomial degree of the basis-functions, h represents the average grid spacing, E is the total number of elements and d is the number of dimensions.

FEM provides an algorithm for solving any well-posed boundary value problem (BVP) and the mathematical formulation is obtained by first finding the Galerkin formulation with a corresponding search space X and then choosing a discrete subspace $X_h^p \subset X$ spanned by the finite element basis functions $\{\phi_i^p\}$. The key property of the basis functions is that they only have local support in a very small part of the domain. This is what gives rise to the resulting sparse linear system. By increasing the polynomial order the number of grid points used to define the polynomial will need to increase as well. This implies either reducing the distance between the grid points or increasing the support of each basis function. Both approaches will reduce the sparsity of the final matrix. Another important aspect of FEM is the treatment of the domain Ω, on which a triangulation $\{\mathcal{T}_h\}$ is defined such that the original domain is divided into elements. By defining a reference element and a general mapping function, all the local contributions can be calculated by a generalized quadrature rule before being added to the global system of equations. This is a process tailored for parallelization, and can be generalized for a wide range of problems.

FEM is called a projection method since the solution $u_h \in X_h^p$ is a projection of the actual solution u of the BVP onto the discrete space X_h^p. Provided that the initial BVP is well-posed there exists two constants $M, \alpha > 0$ known as the bounded and coercivity constant such that the error of the solution can be reduced to a pure projection error.

The result is known as Cea's lemma,

$$||u - u_h||_X \leq \frac{M}{\alpha} \min_{v_h \in X_h^p} ||u - v_h||_X, \tag{3.5}$$

the solution u_h provided by the Galerkin method is known as the orthogonal projection of u onto X_h^p.

Before this section ends it is important to understand the two ways to increase accuracy and the effects these two ways have on the algorithm. Assume the solution of the BVP to be infinitely smooth and the domain be sufficiently regular. This yields an error $e = Ch^p$, being some positive constant. Factors such as geometric complexity, condition-number, non-linear operators and the continuity of the solution will all provide slightly more complicated error estimates. However for a simpler BVP such as the Poisson problem on the unit square, the error estimate is valid. A h-refinement will lead to an algebraic convergence of order p, while the sparsity of the system is conserved and the total algorithm does not change in any other way than increasing the number of elements. Keeping h constant and increasing p will provide spectral convergence, but the sparsity will be reduced and all integrals solved will require quadrature rules of higher order. A formal statement and numerical validation of the error estimate can be found in [7] chapter 2.6.

To sum up the discussion above a general error estimate from [8] is stated as a theorem,

Theorem 3.1. *Let Ω be a domain in $\mathbb{R}^d$ and $\{\Omega_k\}$ be the non-overlapping elements with a corresponding element size h_k. The function u is locally regular within each element, $u_{|\Omega_k} \in H^\sigma(\Omega_k)$. Approximating this function with $u_h \in X_h^p \subset H_0^1$, where X_h^p is the FEM space, yields the following error estimate for $\sigma > p \geq 1$*

$$\inf_{u_h \in X_h^p} ||u - u_h||_1 \leq C \left(\sum_k h_k^{2p} |u|_{p+1,k}^2 \right)^{1/2}. \tag{3.6}$$

3.3   SPECTRAL METHODS

Spectral methods (SM) share a some of the mathematical ideas as FEM, but are not as widely used in real life problems. There are many ways to apply SM, and in this thesis only the Galerkin version with numerical integration (sometimes referred to as G-NI) will be considered and will be referred to only as SM. For a full introduction to SM and its applications to BVP see [12]. SM can be reduced to a interpolation problem such as FEM, and are very interesting from a theoretical point of view due to its spectral convergence rate which allows you to obtain solutions of extremely high accuracy. The most important draw-back of SM are the difficulties with applications to complex geometries. Although the system of equations surging from a BVP can be constructed in an elegant way it is rarely sparse and often result in expensive calculations.

Applying SM on a BVP in one dimension requires a set of basis functions $\{\psi_i\}_N$ defined on the whole domain Ω. The discrete space $X_h(\Omega)$ spanned by the basis functions involves all polynomials up to degree N. A function u is projected onto X_h by the relation

$$u_h(x) = \sum_{i=0}^{N} a_i \psi_i(x). \tag{3.7}$$

Where the coefficients a_i are called the expansion coefficients. There are many possible choices for the basis and the belonging coefficients, in this thesis and the algorithms used the functions ψ_i will be the Lagrange polynomials based on the Gauss-Lobatto-Legendre (GLL) nodes. The reason for choosing these nodes is because it enables us to apply the Gauss-Lobatto quadrature rule. This is one of several existing Gauss-quadratures, and the only one allowing fixed endpoints which is the case for this thesis. For more detailed information on GL-quadrature and other quadrature rules it is referred to [13].

The GLL-nodes $\{\xi_i\}_{N+1}$ are given as the solutions of the equation

$$(1 - \xi^2)L'_N(\xi) = 0. \tag{3.8}$$

L_N being the Legendre polynomial of degree N, defined from the Sturm-Liouville problem

$$\frac{d}{dx}\left[(1-x^2)\frac{d}{dx}L_n(x)\right] + n(n+1)L_n(x) = 0. \tag{3.9}$$

With equations Eq. (3.8) and Eq. (3.9) the local spectral basis functions ψ_j can be stated as

$$\psi_j(x) = \prod_{i\neq j}^{N}\frac{x-x_i}{x_j-x_i}. \tag{3.10}$$

$\{x_i\}$ being the solutions to Eq. (3.8). Note that $\psi_j(x_i) = \delta_{ij}$. The expansion coefficients in Eq. (3.7) are then chosen as $a_i = u_i := u(x_i)$.

This definition of the expansion coefficients is very convenient since the actual value of the function in any point can just be read directly from the coefficients without having to sum all the contributions from the different polynomials. Creating a basis for 2 and 3 dimensions is done simply by taking the tensor product of the basis functions in each direction. In order to keep track of indices in this section $i, j, k = 1, \cdots, N$ is used to keep track of Lagrange polynomials in one direction while $m, l, n = 1, \cdots, N^d$ will be used for the tensor product of the Lagrange polynomials spanning an entire element. for 3 dimensions the basis functions Ψ_l are given as

$$\Psi_l(\mathbf{x}) = \psi_i(x)\psi_j(y)\psi_k(z). \tag{3.11}$$

This expansion to multiple dimensions preserves the $\Psi_l(\mathbf{x}_m) = \delta_{lm}$. In order to clarify some of the concepts the SM approach will be applied on the Helmholtz equation

$$-\Delta u + \lambda u = f \quad \text{in } \Omega, \tag{3.12}$$

$$u = 0 \quad \text{on } \partial\Omega. \tag{3.13}$$

Ω will for this example be defined as the unit square $[-1, 1]^2$. Let us start by defining the space $V = H_0^1(\Omega)$ and assuming $f \in L^2(\Omega)$. The weak formulation after applying the divergence theorem can now be stated.

Find $u \in V$ st.

$$\int_\Omega \nabla u \cdot \nabla v d\Omega + \lambda \int_\Omega uv d\Omega = \int_\Omega fv d\Omega \qquad \forall v \in V \tag{3.14}$$

In order to solve this using SM the discrete space $V_h \subset V$ is defined as span$\{\Psi_l\}$ following the preceding definitions the discrete weak formulation is stated as Find $u_h \in V_h$ st.

$$\sum_l \left(u_l \int_\Omega \nabla \Psi_l \cdot \nabla \Psi_m d\Omega + u_l \lambda \int_\Omega \Psi_l \Psi_m d\Omega \right) = \int_\Omega f \Psi_m d\Omega \qquad \forall \Psi_m \in V_h. \tag{3.15}$$

The following step of this particular spectral method is evaluating the integrals by using the GLL-quadrature rule, the resulting system of equations is then given as

$$\sum_l \left(u_l \sum_n \rho_n \nabla \Psi_l(\mathbf{x}_n) \cdot \nabla \Psi_m(\mathbf{x}_n) + u_l \lambda \sum_n \rho_n \Psi_l(\mathbf{x}_n) \Psi_m(\mathbf{x}_n) \right) \tag{3.16}$$

$$= \sum_n \rho_n f \Psi_m(\mathbf{x}_n) \qquad \forall \Psi_m(\mathbf{x}_n) \in V_h. \tag{3.17}$$

ρ_n is the quadrature weight for the nth node, and $\mathbf{x}_n$ is the vector containing the coordinates to the nth node. Note that all the indices $l, m, n = 1, \cdots, N_x N_y$. This can be written in a compact matrix form as

$$(A + \lambda M)u_h = \tilde{f}. \tag{3.18}$$

Where the elements in the matrices and vectors are given as

$$\begin{aligned} A_{lm} &= \sum_n \rho_n \nabla \Psi_l(\mathbf{x}_n) \cdot \nabla \Psi_m(\mathbf{x}_n), \\ M_{lm} &= \sum_n \rho_n \Psi_l(\mathbf{x}_n) \Psi_m(\mathbf{x}_n) = \rho_l \delta_{lm}, \\ (u_h)_l &= u(\mathbf{x}_l), \\ \tilde{f}_m &= \sum_n \rho_n f(\mathbf{x}_n) \Psi_m(\mathbf{x}_n) = \rho_m f(\mathbf{x}_j). \end{aligned} \tag{3.19}$$

From these equations it is clear that the mass matrix M is diagonal and the right hand side vector $\tilde{f}$ is easily calculated, while the stiffness matrix A is symmetric but full.

The method oulined in this section is similarly to FEM also a projection method, but by applying a different set of basis functions the projection error is different as well.

Theorem 3.2. *Let $\Omega \subset \mathbb{R}^d$ and $u \in H^\sigma(\Omega)$. The projection of u onto $\mathbb{P}_N$ for any $\sigma \geq 1$ is given as*

$$\inf_{u_h \in P_N} ||u - u_h||_1 \leq CN^{1-\sigma}|u|_\sigma. \tag{3.20}$$

3.4 Spectral element method

In the early 1980's the idea to combine FEM and SM came along in order to obtain the flexibility and sparse properties of FEM combined with the spectral convergence rate provided by SM. The result was the Spectral element method (SEM). Several formulations were investigated mainly by Patera and Maday in the papers [14], [15], [16] with important contributions from Fischer, Rønquist and several more. It is important to understand that when solving the N-S equations the efficiency of the solution method is crucial. The algorithm has to be parallelizable and the development of the super-computers and computational clusters has played an important role in deciding which variants of SEM is applied today. The idea is to divide the domain of the BVP into elements as in FEM and then use spectral basis functions of higher degree with support only within one single element.

In the previous subsection the power of spectral methods was illustrated on the unit square in two dimensions. But the limitations when it comes to more complex geometry rapidly affects the spectral convergence rate. Let $\hat{\Omega}$ be the reference element $[-1, 1]^d$, the standard procedure when working on a deformed geometry Ω with SM is to first create a map $\mathcal{F} : \hat{\Omega} \to \Omega$. An example of this map is the Gordon-Hall procedure described in Chapter 3.4.4. The Jacobian is then given as the transposed tensor derivative of $\mathcal{F}$, which in two dimension is written as

$$\mathbf{J} = (\nabla \otimes \mathcal{F})^T = \begin{bmatrix} \frac{\partial \mathcal{F}_1}{\partial x} & \frac{\partial \mathcal{F}_1}{\partial y} \\ \frac{\partial \mathcal{F}_2}{\partial x} & \frac{\partial \mathcal{F}_2}{\partial y} \end{bmatrix}, \qquad J = \det(\mathbf{J}). \tag{3.21}$$

This allows us to transform both derivatives and integrals to the reference domain, let $\boldsymbol{\xi} = [\xi, \eta]^T$ denote the axis in the reference domain corresponding to $\mathbf{x} = [x, y]^T$ in the

deformed domain. The transformation is performed according to the following identities

$$d\mathbf{x} = \mathbf{J}d\boldsymbol{\xi}$$

$$\int_{\Omega} f(\mathbf{x})d\mathbf{x} = \int_{\hat{\Omega}} \hat{f}Jd\boldsymbol{\xi} \tag{3.22}$$

$$\nabla u = \mathbf{J}^{-T}\hat{\nabla}\hat{u}.$$

Here $\hat{u}$, $\hat{f}$ are obtain by simply substituting $\mathbf{x}$ with $\mathcal{F}(\boldsymbol{\xi})$ and $\hat{\nabla}$ is the partial differential operator wrt. $\boldsymbol{\xi}$. The important thing to notice here is that whenever an integral is solved and a derivative is introduced the Jacobian appears in the equation. When applying the GLL-quadrature to solve the integrals, equality is guaranteed if and only if the function integrated is of polynomial degree $2n - 1$ or less, and the error gets bigger with increasing polynomial degree. A higher order Jacobian could imply a large error in the quadrature.

Although the whole domain Ω is deformed, the deformation of each element $\{\Omega_k\}$ is normally a lot less crucial. This gives SEM a huge advantage and allows it to obtain accurate results even in complicated domains.

Let us again consider the Helmholtz problem Eq. (3.13), but this time on a more general domain Ω. The set of elements $\{\Omega_k\}$ is defined such that $\Omega_i \bigcap \Omega_j$ is either empty, a vertex or a line and $\Omega = \bigcup_{k=1}^{K} \Omega_k$. By applying SEM to Eq. (3.13) the corresponding weak formulation can be stated.

For all elements Ω_k Find $u_{h,k} \in X_k^N$ such that

$$\int_{\Omega_k} \nabla u_{h,k} \cdot \nabla v_{h,k}d\Omega + \lambda \int_{\Omega_k} u_{h,k}v_{h,k}d\Omega = \int_{\Omega_k} fv_{h,k}d\Omega \qquad \forall v_{h,k} \in X_k^N. \tag{3.23}$$

Where $X_k^N = H_0^1(\Omega_k) \bigcap \mathbb{P}_N(\Omega_k)$. The same discretization procedure as performed for the pure spectral case is now done for each of the sub-domains Ω_k,

$$\sum_i \left(u_i \int_{\Omega_k} \nabla \psi_i \cdot \nabla \psi_j d\Omega + u_i \lambda \int_{\Omega_k} \psi_i \psi_j d\Omega \right) = \int_{\Omega_k} f\psi_j d\Omega \qquad \forall \psi_j \in V_h. \tag{3.24}$$

Since the elements can be deformed a Gordon-Hall map is constructed to map the coordinates to the reference element $\hat{\Omega} = [-1, 1]^d$. Applying the identities from Eq. (3.22)

to Eq. (3.24) yields

$$\sum_i \left(u_i \int_{\hat{\Omega}_k} (\mathbf{J}^{-T}\hat{\nabla}\hat{\psi}_i)^T (\mathbf{J}^{-T}\hat{\nabla}\hat{\psi}_j) J d\hat{\Omega} + u_i\lambda \int_{\hat{\Omega}_k} \hat{\psi}_i\hat{\psi}_j J d\hat{\Omega} \right) = \int_{\hat{\Omega}_k} \hat{f}\psi_j J d\hat{\Omega} \qquad \forall \psi_j \in V_h.$$

$$\sum_i \left(u_i \int_{\hat{\Omega}_k} \hat{\nabla}^T\hat{\psi}_i \mathbf{J}^{-1}\mathbf{J}^{-T}\hat{\nabla}\hat{\psi}_j J d\hat{\Omega} + u_i\lambda \int_{\hat{\Omega}_k} \hat{\psi}_i\hat{\psi}_j J d\hat{\Omega} \right) = \int_{\hat{\Omega}_k} \hat{f}\psi_j J d\hat{\Omega} \qquad \forall \psi_j \in V_h.$$

$$(3.25)$$

Notice how the integrals depend on the Jacobian $\mathbf{J}$ and its determinant J. The local matrices A_k, M_k and the loading vector f_k are gathered from each element. Equivalently as for FEM the global matrices has to be assembled from all the local matrices corresponding to each sub-domain. This procedure is general and if the elements are chosen to be sufficiently small it can be performed on almost any deformed domain as opposed to SM.

3.4.1 CONVERGENCE PROPERTIES

This subsection will present a brief error estimate which in can be compared to Theorem 3.1 and 3.2. The Spectral Element Method can as mentioned earlier be regarded as a projection method similar to FEM and SM. It was proved in [17] that spectral convergence can be achieved only by requiring the solution u to be sufficiently regular within each element. This as opposed to pure spectral methods which requires regularity in the entire domain is an advantage when working with turbulent flows in complex domains. Let $\mathbb{P}_{N,K} = \left\{ v \in L^2(\Omega), v_{|\Omega_k} \in \mathbb{P}_N(\Omega_K) \right\}$.

Theorem 3.3. *Let Ω be a domain in $\mathbb{R}^d$ and $\{\Omega_k\}$ be the set of non-overlapping elements. $X_h = H_0^1 \cap \mathbb{P}_{N,K}$ is the SEM space. If u is continuous in the entire domain and $u_{|\Omega_k} \in H^\sigma(\Omega_k) \forall\, k$ the following will hold for any $\sigma \geq 1$*

$$\inf_{v_h \in X_k} ||u - v_h||_1 \leq C N^{1-\sigma} \left(||u||_1 + \sum_{k=1}^K ||u||_{\sigma,k} \right). \qquad (3.26)$$

Note that this result is for a spatial approximation of a function u, although SEM provides great error estimates the solution of the N-S equations are also restricted by the errors due to temporal discretizations. This will be further discussed in Chapter 3.5.

3.4.2 FILTERING

Although SEM provides spectral convergence in space, a non-sufficient resolution of the smallest structures often leads to spurious nodes and an unstable scheme as shown in chapter 2.4.1.2 in [7]. In [18] a filter-based stabilization is introduced for SEM applied on the Navier-Stokes equations. The idea is to project a part $0 < \alpha < 1$ of the of the solution onto a polynomial space of lower order, explicitly they define the filter F_α as

$$F_\alpha = \alpha I_{N-1} + (1 - \alpha)I_d. \tag{3.27}$$

Where I_{N-1} is the projector from $\mathbb{P}_N$ to $\mathbb{P}_{N-1}$ and I_d is the identity operator. The parameter α is recommended to be somewhere in the interval $(0.05, 0.3)$.

The effect of F_α in Legendre space is analysed by Pasquetti and Xu in [19]. A quick demonstration of how the filter works will however be given here.

Let $u = \sum_{i=0}^{N} \hat{u}_i L_i$ be the solution to some PDE, where L_i denote the Lagrange polynomial of order i and $\hat{u}_i$ the corresponding coefficient. The effect of the filter can be given as

$$F_\alpha u = (1 - \alpha)\hat{u}_N L_N + \hat{u}_{N-1} L_{N-1} + (\hat{u}_{N-2} + \alpha\hat{u}_N)L_{N-2} + \sum_{i=0}^{N-3} \hat{u}_i L_i. \tag{3.28}$$

From this identity the effect of the filter becomes clear, it is simply removing a part α from the highest order mode N to the mode $N - 2$. The rest of the coefficients remain unchanged. For a full derivation and discussion on this matter it is referred to chapter 6.5.1 in [7].

The filter in Eq. (3.28) is in this thesis applied such that the k highest Legendre modes are dampened with coefficients $\alpha_i = (\frac{k+1-i}{k+1})^2 \alpha_0$. With α_0 being the filter constant for the highest mode. The action of the filter can therefore be described as a matrix equation in two steps, first adding the contribution from the higher polynomials to the lower ones and then subtracting the contribution from the higher polynomials. Let u be the vector containing the Legendre coefficients.

$$\begin{aligned} u^* &= (I + \mathcal{F}_\alpha)u, \\ u^{**} &= (I - I_{\alpha,k})u^*. \end{aligned} \tag{3.29}$$

In this case $I_{\alpha,k}$ is a diagonal matrix $\text{diag}(0, 0, \cdots, \alpha_k, \alpha_{k-1}, \cdots, \alpha_1)$ while $\mathcal{F}_\alpha$ is also sparse and with the same non-zero entries as $I_{\alpha,k}$, but this time they are located on the second sup-diagonal (removing the 2 first zeros). In this thesis the α_k follows a quadratic decay from 1 to k.

The filter is proved to be a very effective stabilization method and it preserves the spectral convergence rate. Another interesting property is that the filtering procedure does not imply dissipation of energy, let the energy norm be defined as $E(u) = ||u||_{L_2}^2$. By applying Parseval's identity [20] the difference in energy between the original solution and the filtered solution is given as

$$\epsilon = E(u) - E(F_\alpha u) \tag{3.30}$$

$$= 2\alpha \hat{u}_N (\hat{u}_N ||L_N||^2 + \hat{u}_{N-2} ||L_{N-2}||^2) - \alpha^2 \hat{u}_N^2 (||L_N||^2 + ||L_{N-2}||^2) \tag{3.31}$$

$$\approx \frac{2\alpha}{N} \left[(1 - \frac{\alpha}{2}) \hat{u}_N^2 + \hat{u}_N \hat{u}_{N-2} \right], \tag{3.32}$$

which can take both positive and negative values depending on the sign and size of $\hat{u}_N \hat{u}_{N-2}$. By applying the known norm of the Legendre polynomials the deduced absolute error ϵ of the filtered energy is of order $\epsilon \sim \alpha/N$. The approximation $||L_N||^2 \approx ||L_{N-2}||^2 \approx 1/N$ have been used to achieve the result in Eq. (3.32).

3.4.2.1   A PHYSICAL APPROACH TO THE FILTER

A good physical description of the filter has not yet been described, this subsection is an attempt to show the resemblance between known properties of some differential equations and the mathematical filter described in the previous section.

Let u be some smooth continuous function, $\bar{u} = [u_1 L_1(x), u_2 L_2(x), \cdots]$ is the corresponding Legendre basis with appropriate coefficients such that $u = sum(\bar{u})$ and P_k is the diagonal matrix with ones on the k last entries and 0 on the rest.

Let us consider the two initial value problems

$$\begin{aligned} \frac{\partial v}{\partial t} &= \Delta v, & v(0) &= v_0, \\ \frac{\partial u}{\partial t} &= -u, & u(0) &= u_0. \end{aligned} \tag{3.33}$$

The second IVP in Eq. (3.33) has a known analytical solution $u = u_0 e^{-t}$ which decays exponentially in time. The first IVP is known as the heat equation and is known to diffuse the initial condition with time. Now let the operators -1 and Δ on the right hand sides of Eq. (3.33) be applied only on the k highest Legendre polynomials. By applying the Legendre decomposition and the truncated operators the system can then be written as

$$
\begin{aligned}
\frac{\partial \bar{v}}{\partial t} &= \Delta P_k \bar{v}^T, & v(0) &= v_0, \\
\frac{\partial \bar{u}}{\partial t} &= -P_k \bar{u}^T, & u(0) &= u_0.
\end{aligned}
\tag{3.34}
$$

The Laplace operator applied in a Legendre space is known to take a sparse upper triangular form with entries only on even sup-diagonals. By naming this matrix A the entries are given as

$$
A_{ij} = 4||L_i||^{-2} \sum_{k=1}^{(j-i)/2+1} ||L_{j+1-2k}||^{-2}, \qquad \text{if } 2 \leq j - i = mod(2).
\tag{3.35}
$$

This relation is derived in A.1.

The matrix-matrix product AP_k will lead to a Laplacian matrix where the $N - k$ first columns are zero while the last k remains unchanged. This modified Laplacian will be denoted A^*. Omitting the initial conditions, and doing a first order implicit Euler of Eq. (3.34) can be written as

$$
\begin{aligned}
(I - \Delta t A^*)u^{n+1} &= u^n \implies u^{n+1} = (I - \Delta t A^*)^{-1} u^n, \\
(I + \Delta t P_k)u^{n+1} &= u^n \implies u^n = (I + \Delta t P_k)^{-1} u^n.
\end{aligned}
\tag{3.36}
$$

Notice the resemblance to the application of the filter in Eq. (3.29). The second step is identical if $\alpha_i = \Delta t/(1 + \Delta t)$. The truncated Laplacian A^* is not equal to the corresponding filter matrix $\mathcal{F}_\alpha$, but there are some similarities between these to matrices. They are both upper triangular with zeros along the diagonal and positive entries on the second sup-diagonal. The main difference is that the Laplacian applied on the Nth Legendre function L_N affect all the terms $L_{N-2}, L_{N-4}, \cdots$, while the filter only affects L_{N-2}. In order to illustrate this effect Figure 3.1 shows the non-zero entries of the Laplacian matrix, the red dots indicate the non-zero entries that are not present in the filtering matrix. If one were to insist that the Laplacian should work locally in Legendre
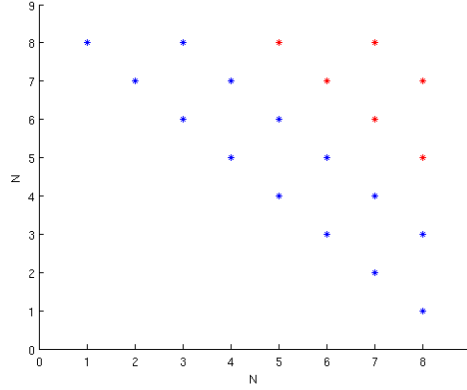
FIGURE 3.1: *The non-zero entries of the Laplacian matrix applied on the last eight Legendre modes. The blue dots are present in both the Laplacian matrix and the filter matrix while the red dots are only non-zero for the Laplacian.*

space, in other words if $A_{ij} = 0$ if $i - j > 2$, then the Laplacian and the filtering would have the same non-zero entries and a clever choice of α_i would yield equality. Notice in particular the similarity of applying a filter and including a SGS-model, with ν_T as a constant in Eq. (2.27) the term $\nabla \nu_T s_{ij}$ reduces to $\nu_T \Delta \mathbf{u}$.

This way of considering the filtering procedure is very similar to the variational multiscale (VMS) approach to LES first introduced by Hughes [21]. This method is based on the assumption that the unresolved structures have a negligible effect on the larger scales, hence the SGS-model is only included for the small but still resolved scales of motion.

3.4.3 ALIASING

When evaluating the integral surging from the non-linear term in the N-S equations the polynomial to be integrated can be of order $2N + (N - 1)$ or even higher depending of the jacobian. The quadrature rule applied to solve the integrals are only exact up to an order $2N - 1$ hence the error surging from this evaluation can be of significant size. Applying a non-sufficient quadrature to an integral like this is called a "variational crime". Applying a quadrature rule of a not sufficiently high order results in an aliasing effect of the lower modes, attempting to compensate for the higher order modes omitted. Since a spectral element method arguably has a good accuracy these variational crimes should not be committed and it is therefore common practice to solve this particular integral using a quadrature of order $3N$. The concept and illustrative examples are given in Chapter 2.4 in [7]. It is worth to note that aliasing is not always a necessity depending

on the size of the smallest structures compared to the grid resolution, an example of this is presented in Chapter 6. This is one of the time vs. accuracy questions one have to decide for each problem. instead of applying the GLL-quadrature "designed" for the basis-functions the functions has to be evaluated in a new set of GLL-points with $3/2$ as many nodes. This is a costly process and should only be applied when absolutely necessary.
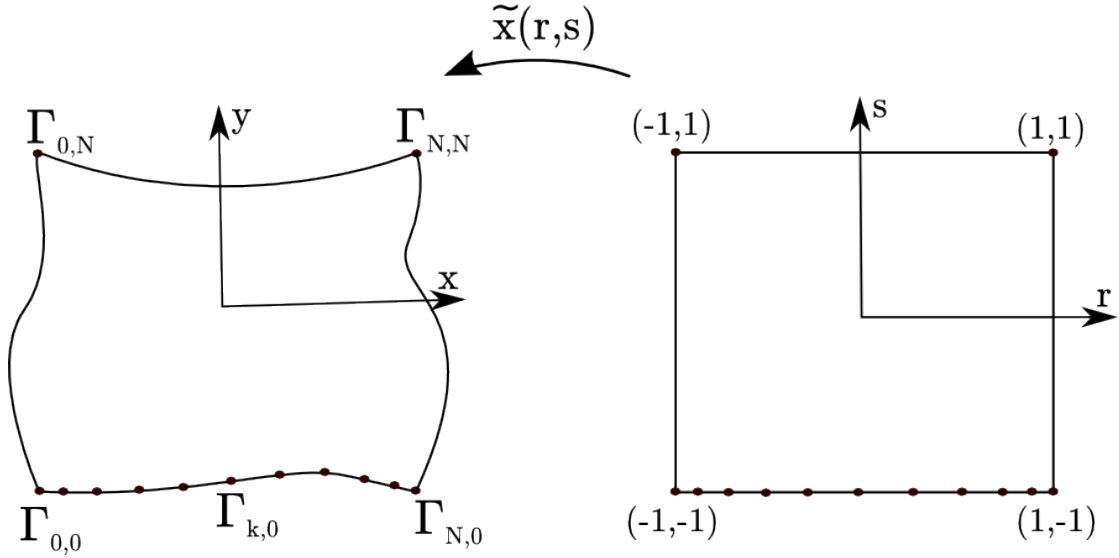
3.4.4 Gordon-Hall algorithm

FIGURE 3.2: *An illustration of how the Gordon-Hall algorithm creates a map from the reference element to the deformed element. The GLL-points are drawn along the edge $\Gamma_{k,0}$ on the deformed element which corresponds to $s = -1$ on the reference element.*

In order to work on complex geometries some elements require a certain deformation in order to be able to describe the entire domain. It is necessary to evaluate all the integrals surging from the weak formulation over a reference domain $\hat{\Omega} = [-1, 1]^d$ for sakes of efficiency and implementation purposes. The Gordon-Hall algorithm is a general method that creates an isometric map from an arbitrary simply connected domain to $\hat{\Omega}$. Let $\tilde{\mathbf{x}}$ be the mapping function from the reference domain to the physical domain given on the form

$$\tilde{\mathbf{x}} = \sum_i \sum_j \sum_k \mathbf{x}_{ijk} l_i(r) l_j(s) l_k(t). \tag{3.37}$$

l_i being the ith Lagrange polynomial. The full description of the algorithm with helpful figures can be found in [22] chapter 4. Without going to much into the mathematical foundation of this method a more intuitive and implementable presentation of the method will be provided in this chapter. For simplicity a two-dimensional domain will be considered here, and the 3D case will be an easy expansion of the algorithm presented here. Consider a deformed domain $\Omega \in \mathbb{R}^2$ (Figure 3.2), with $\Gamma_{i,j}$ representing the discrete boundary coordinates. The four vertices can then be expressed as $\Gamma_{0,0}, \Gamma_{0,N}, \Gamma_{N,0}\Gamma_{N,N}$. Let ϕ_0, ϕ_N be defined as

$$\phi_0(\xi) = \frac{1-\xi}{2}, \qquad \phi_N(\xi) = \frac{1+\xi}{2}. \tag{3.38}$$

Let $\{\xi_0, \ldots, \xi_N\}_{N+1} = \{-1, \ldots, 1\}_{N+1}$ be the GLL-points corresponding to the Lagrange polynomial of order N. An important property for the functions in Eq. (3.38) is that $\phi_0(\xi_0) = \phi_N(\xi_N) = 1$ and $\phi_0(\xi_N) = \phi_N(\xi_0) = 0$.

The algorithm provides a stepwise routine depending on the complexity of the domain. The first step is to create a mapping to a polygon spanned from the vertices of Ω.

$$\begin{aligned}
\tilde{\mathbf{x}}_{i,j} = {}& \Gamma_{0,0}\phi_0(r_i)\phi_0(s_j) \\
& + \Gamma_{0,N}\phi_0(r_i)\phi_N(s_j) \\
& + \Gamma_{N,0}\phi_N(r_i)\phi_0(s_j) \\
& + \Gamma_{N,N}\phi_N(r_i)\phi_N(s_j)
\end{aligned} \tag{3.39}$$

If the edges are straight the algorithm ends here, but for curved edges a second step is performed adding the deformation of the edges.

$$\begin{aligned}
\tilde{\mathbf{x}}_{i,j} = {}& \tilde{\mathbf{x}}_{i,j} + (\Gamma_{i,0} - \tilde{\mathbf{x}}_{i,0})\phi_0(s_j) \\
& + (\Gamma_{i,N} - \tilde{\mathbf{x}}_{i,N})\phi_N(s_j) \\
& + (\Gamma_{0,j} - \tilde{\mathbf{x}}_{0,j})\phi_0(r_i) \\
& + (\Gamma_{N,j} - \tilde{\mathbf{x}}_{N,j})\phi_N(r_i)
\end{aligned} \tag{3.40}$$

In 3D the additional knowledge of the faces may be applied to create mappings from elements with deformed faces as a third step. The only difference when applying this algorithm in three dimensions is that you need to include ϕ for a third coordinate t_k and the number of vertices, and edges are 8 and 12 instead of 4 and 4.

3.5   Time integration for incompressible N-S

So far the spatial discretization by SEM has been described in detail and so far been proved to yield spectral convergence, but for unsteady flows the development in time is determined by the temporal discretization and puts an additional restriction on the convergence rate. Because the N-S equations are very computationally demanding to solve exactly a large number of splitting methods have been developed, all attempting to find the ideal balance between speed and accuracy. The most common set of solution methods are called projection methods, which first calculates a velocity field that does not fulfill the divergence free condition and then projecting this field onto a divergence free space. For an extensive discussion regarding projection methods it is referred to [23]. The projection is done by solving a Poisson equation for the pressure (PPE).

3.5.1   Operator-splitting techniques

In this chapter a_j, b_j will denote the coefficients for some explicit and implicit scheme. Let us consider a simplified transient problem

$$\frac{du}{dt} = f(u,t)u + g(t)u. \tag{3.41}$$

f is here a function of u and t, while g is only dependent of the time t. Let superscript denote the timestep, such that $g^n = g(n\Delta t)$ for some fixed timestep Δt. One step applying a kth order Backward Difference scheme (BDFk) yields

$$\sum_{j=0}^{k} b_j u^{n+1-j} = \Delta t f^{n+1} u^{n+1} + \Delta t g^{n+1} u^{n+1}. \tag{3.42}$$

Now notice that $f^{n+1} = f(u^{n+1}, t^{n+1})$ requires that u is known at time t^{n+1} which is not achievable at the current step. This term is therefore approximated by a kth order explicit scheme leading to

$$\sum_{j=0}^{k} b_j u^{n+1-j} = \Delta t \sum_{j=0}^{k} a_j f^{n-j} u^{n-j} + \Delta t g^{n+1} u^{n+1}. \tag{3.43}$$

Now the terms can be ordered such that only the implicit terms are present on the left hand side,

$$(b_0 - \Delta t g^{n+1}) u^{n+1} = -\sum_{j=1}^{k} b_j u^{n+1-j} + \Delta t \sum_{j=0}^{k} a_j f^{n-j} u^{n-j}. \qquad (3.44)$$

This way of solving Eq. (3.41) allows easy invertible terms to be solved implicitly while non-linear terms can be extrapolated. In the Navier-Stokes equation this strategy will be applied to split the non-linear term from the rest. In this thesis the schemes BDFk and a kth order extrapolation (EXTk) for $k = 2, 3$ are applied, the coefficients can be found in [24].

It should be mentioned that the explicit/implicit schemes introduced in this section are stable only for operators with eigenvalues below a certain limit γ that depends on the scheme. When applied on the N-S equations it is the convection term $\Delta t M^{-1} C \mathbf{u}^{n+1}$ as observed in Eq. (3.55) that is evaluated by an explicit scheme. Let λ_{max} be the maximum eigenvalue of $M^{-1}C$, which is known to scale as $\mathcal{O}(N^2) = \mathcal{O}(\Delta x_{\min}^{-1})$. The following inequality has to be satisfied for the scheme to be stable,

$$\Delta t \lambda_{\max} = c \frac{\Delta t}{\Delta x} \leq \gamma. \qquad (3.45)$$

By introducing the Courant number, $\text{CFL} = \bar{u} \Delta t / \Delta x$, and a discretization-specific constant S, the inequality in Eq. (3.45) can be rewritten as the CFL-condition,

$$S \cdot \text{CFL} \leq \gamma. \qquad (3.46)$$

This inequality is used to adjust the time-step in order to maximize the evolution in time within the stability criteria for the scheme.

3.5.2 Operator integrating factor schemes (OIFS)

The operator-splitting method described in the previous chapter may lead to an unstable scheme, and require very small time-steps. OIFS is a similar method but it offers a more stable scheme and is more efficient by using a multi-step method that allows larger advances in time. The presentation of the method is presented here in a computational

fashion, for a full description and derivation of the method it is referred to Maday et al [25].

Throughout this section the NS-equation will be considered in its operational form as introduced in 2.14

$$M\frac{d\mathbf{v}}{dt} + C\mathbf{v} = -A\mathbf{v} + D^T p + M\mathbf{f}, \qquad D\mathbf{v} = 0 \tag{3.47}$$

Now let $Q(t)$ be an operator such that $Q(t^{n+1}) = I$ and

$$\frac{dQ(t)M\mathbf{v}}{dt} = Q(t)M\frac{d\mathbf{v}}{dt} + \frac{d}{dt}\left[Q(t)M\right]\mathbf{v}, \tag{3.48}$$

$$= Q(t)M\frac{d\mathbf{v}}{dt} + Q(t)C\mathbf{v}. \tag{3.49}$$

This way Eq. (3.47) can be written as

$$\frac{dQ(t)M\mathbf{v}}{dt} = Q(t)(-A\mathbf{v} + D^T p + M\mathbf{f}). \tag{3.50}$$

Evaluating this equation with a BDFk-scheme results in a system

$$\sum_{j=0}^{k} b_j Q(t^{n+1-j})M\mathbf{v}^{n+1-j} = \Delta t\, Q(t^{n+1})(-A\mathbf{v}^{n+1} + D^T p^{n+1} + M\mathbf{f}^{n+1}). \tag{3.51}$$

Applying the fact that $Q(t^{n+1}) = I$ enables Eq. (3.52) to be written as

$$b_0 M\mathbf{v}^{n+1} + \sum_{j=1}^{k} b_j Q(t^{n+1-j})M\mathbf{v}^{n+1-j} = \Delta t(-A\mathbf{v}^{n+1} + D^T p^{n+1} + M\mathbf{f}^{n+1}). \tag{3.52}$$

Notice how all the easily invertible operators are evaluated implicitly, while the convective non-linear term is hidden in the BDFk scheme. OIFS allows the terms in the sum to be calculated in a rather elegant fashion. First of all the auxiliary variable $\tilde{\mathbf{v}}_j$ is defined such that $Q(t^{n+1-j})M\mathbf{v}^{n+1-j} = M\tilde{\mathbf{v}}_j$ thus enabling the summation expression to be found by solving the initial value problem

$$M\frac{d\tilde{\mathbf{v}}_j}{ds} = -C(\tilde{\mathbf{v}}_j(s))\tilde{\mathbf{v}}_j(s), \qquad t^{n+1-j} \le s \le t^{n+1}$$
$$\tilde{\mathbf{v}}_j(t^{n+1-j}) = \mathbf{v}(t^{n+1-j}). \tag{3.53}$$

Notice how the integrational factor $Q(t)$ is never evaluated directly.

The final scheme applied for solving Eq. (3.47) when applying OIFS consists of one implicit scheme for solving Eq. (3.52) and an explicit scheme for solving Eq. (3.53). When applied in this thesis the first scheme corresponding to the b_j coefficients is an implicit BDFk-scheme while the second is an explicit 4th order Runge-Kutta scheme (RK4). Solving Eq. (3.53) with a multi-step method implies a bit more work per time-step, but as it stabilizes the routine larger advances in time can be made and the overall efficiency improves.

3.5.3 FRACTIONAL STEP - $(P_N P_N)$

Fractional step is an algorithm that can be divided into four separate steps. The N-S equations will still be considered in its operational form

$$M\frac{d\mathbf{u}}{dt} + C\mathbf{u} = -A\mathbf{u} + D^T p + M\mathbf{f}. \tag{3.54}$$

Where M, A, D, C Denotes the mass integral, Laplacian, gradient and non-linear operator. A schematic overview of the method is stated below, where the equations on the right hand side are solved and the updated solution is stated on the left hand side. By performing these steps the solution $(\mathbf{u}, p)$ is developed one time-step from $(\mathbf{u}^n, p^n)$ to $(\mathbf{u}^{n+1}, p^{n+1})$.

$$
\begin{aligned}
\mathbf{u}^* &= -\sum_{j=1}^{k} b_j \mathbf{u}^{n+1-j} + \Delta t M^{-1}(C\mathbf{u}^{n+1} + M\mathbf{f}^{n+1}), \\
\Delta p^{n+1} &= \nabla \cdot \left(\frac{\mathbf{u}^*}{\Delta t}\right), \\
\mathbf{u}^{**} &= \mathbf{u}^* + \Delta t M^{-1} D^T p^{n+1}, \\
b_0 \mathbf{u}^{n+1} &= \mathbf{u}^{**} - \Delta t M^{-1} A\mathbf{u}^{n+1}.
\end{aligned}
\tag{3.55}
$$

As earlier mentioned this method is convenient because it allows us to handle the different terms with different solution techniques. Hence the term including the non-linear skew-symmetric advection matrix C will be approximated by an kth order extrapolation (EXTk) scheme. The first step can also be evaluated in an OIFS-way to gain stability. This implies using the discretization introduced in Eq. (3.52) with only the loading function on the right hand side, and solving the IVP Eq. (3.53) with RK4 to obtain $\mathbf{u}^*$.

The second equation is the Poisson pressure equation which assures a divergence free velocity field, and it is this step along with step three that allows this to be classified as a projection method.

Note that $p \in L^2 \supset H^1$ hence the Poisson equation is somewhat different from the one normally studied in textbooks. Another difficulty is the treatment of the boundary conditions. Ideally the BC's should be determined by the velocity field $\mathbf{u}^{n+1}$, but since this solution is yet to be calculated the intermediate velocity field $\mathbf{u}^*$ is used to impose the boundary conditions. With p^{n+1} known the third equation is simply an update of the velocity in order to impose the divergence free condition. Now the last equation is solved implicitly due to its nice symmetric structure. This results in a system equivalent to the Helmholtz problem which will be discussed in detail in Chapter 3. This can be easily shown by discretizing the equation,

$$
\begin{aligned}
(\mathbf{u}^{n+1} - \mathbf{u}^n)/\Delta t &= -A\mathbf{u}^{n+1}, \\
A\mathbf{u}^{n+1} + \frac{1}{\Delta t}\mathbf{u}^{n+1} &= \mathbf{u}^n.
\end{aligned}
\tag{3.56}
$$

Knowing that A is the discrete Laplacian and $\mathbf{u}^n$ is a known variable this is similar to problem Eq. (3.13).

This method provides an efficient algorithm, but is known to produce errors of order $\mathcal{O}(1)$. The problem is the pressure Poisson equation which is solved with incorrect boundary conditions.

3.5.4 Discrete splitting - $(P_N P_{N-2})$

The fractional step method is a splitting method based on the idea that two analytical operators can be applied in sequence and still provide a good result. The method presented in this section makes no such assumption and splits the discrete system of equation instead of applying the operators in sequence. The algorithm presented here is similar to the Uzawa algorithm, but with some adjustments to make it more efficient. The detailed description regarding the implementation in Nek5000 is found in [26].

To start the explanation of the method we continue considering the incompressible N-S equations in their operational form

$$\frac{1}{\Delta t}M\mathbf{u}^{n+1} - D^T p^{n+1} + A\mathbf{u}^{n+1} = M\tilde{\mathbf{f}}^{n+1}, \qquad D\mathbf{u}^{n+1} = 0. \tag{3.57}$$

The outline of the method is based on Eq. (3.3), but with some changes. Since this is a method for the unsteady N-S equation the time derivative has to be included, and the non-linear term which is treated explicitly as studied in Chapter 3.5.1 and 3.5.2 is added as a part of the right hand side function. So $M\tilde{\mathbf{f}}^{n+1}$ does in this equation incorporate both the original loading function, the non-linear term and the explicit part of the time-derivative from the BDFk-scheme. By doing this reformulation the unsteady Stokes problem is obtained and algorithms studied for this problem can be applied. By defining the matrix $H = 1/\Delta t M + A$ Eq. (3.57) can be written as

$$\begin{pmatrix} H & -D^T \\ D & 0 \end{pmatrix} \begin{pmatrix} \mathbf{u}^{n+1} \\ p^{n+1} \end{pmatrix} = \begin{pmatrix} M\tilde{\mathbf{f}}^{n+1} \\ 0 \end{pmatrix}. \tag{3.58}$$

It is convenient for the splitting that will be done in the next step to introduce the pressure difference $\delta p^{n+1} = p^{n+1} - p^n$. Eq. (3.59) can be restated as

$$\begin{pmatrix} H & -D^T \\ D & 0 \end{pmatrix} \begin{pmatrix} \mathbf{u}^{n+1} \\ \delta p^{n+1} \end{pmatrix} = \begin{pmatrix} M\tilde{\mathbf{f}}^{n+1} + D^T p^n \\ 0 \end{pmatrix}. \tag{3.59}$$

Solving this exactly is known as the Uzawa algorithm and is known to be computationally demanding and converge slowly. To overcome this issue simplifications and reformulations are made which saves a lot of computational time at the cost of accuracy. The system is rewritten using a LU-factorization of the matrix in Eq. (3.59), which will allow the solution to be found in two separate steps. This requires the inverse of H that will be replaced by an approximation $Q \approx H^{-1}$. The matrix decomposition is given as

$$\begin{pmatrix} H & -D^T \\ D & 0 \end{pmatrix} \approx \begin{pmatrix} H & 0 \\ -D & -DQD^{-1} \end{pmatrix} \begin{pmatrix} I & -QD^T \\ 0 & I \end{pmatrix}. \tag{3.60}$$

Applying these two matrices leads to a two step algorithm on the form

$$\begin{pmatrix} H & 0 \\ -D & -DQD^{-1} \end{pmatrix} \begin{pmatrix} \mathbf{u}^* \\ \delta p^{n+1} \end{pmatrix} = \begin{pmatrix} M\mathbf{f}^{n+1} + D^T p^n \\ 0 \end{pmatrix}, \tag{3.61}$$

$$\begin{pmatrix} I & -QD^T \\ 0 & I \end{pmatrix} \begin{pmatrix} \mathbf{u}^{n+1} \\ \delta p^{n+1} \end{pmatrix} = \begin{pmatrix} \mathbf{u}^* \\ \delta p^{n+1} \end{pmatrix} \tag{3.62}$$

In order to clarify what is actually going on a brief description of each step is given, The first step in Eq. (3.61) corresponds to an initial solution of the velocity using the old pressure value, notice that this will not guarantee a divergence free velocity. The second step in Eq. (3.61) is referred to as the discrete pressure Poisson equation and will make sure that the pressure corresponds to a divergence free flow. When solved in practice the velocity used in this equation is the updated velocity from the first step. This way of updating the pressure is the reason why this method is often referred to as a pressure correction method. The first step in Eq. (3.62) is just a projection of the velocity field onto a divergence free space. The final step is of no real value and will instead be replaced by an update of the pressure $p^{n+1} = p^n + \delta p^{n+1}$.

In this thesis the approximation of the inverse Helmholtz matrix was of first order, $Q = \Delta t M^{-1}$. It is possible to make higher order approximations, but this is a very convenient definition since M is a diagonal matrix.

Unlike the fractional step method this way of solving the N-S equations requires the discrete spaces for velocity and pressure to meet the inf-sup condition stated in Eq. (3.4). It also induces a discrete splitting error. The splitting error induced by this scheme has been a topic of discussion for many years, see for instance the discussion between Perot and Abdallah in [27], [28] and [29]. The author will not choose sides in this debate, but rather state that there will be some numerical differences between these two methods which will be presented in Chapter 6.

It is however apparent from the treatment of the pressure that this yields an algorithm that works well for steady flows. Notice that the error surging from the splitting in Eq. (3.60) is proportional to δp^n instead of p^n as it would be for a straight forward derivation. The method yields a second order scheme as proved by [30], provided that the time discretization is of the same or higher order.

CHAPTER 4

APPLICATION OF NEK5000

There are many numerical solvers for turbulent flows available on the market. From large commercial softwares such as Fluent which runs as a black-box solver, to full open-source codes such as Nek5000 and openFOAM. The solvers can vary in the numerical method; Finite volume, Finite Differences, Finite Element Method, Spectral Element Method etc., The particular algorithm for resolving the Pressure-Velocity coupling, for instance Fractional Step, Poisson pressure and Uzawa. The type of simulation available also varies from solver to solver, whether they apply RANS, LES, DNS or a variety of these. Although most solvers offer multiple of the settings listed above it is important to be aware of their strengths and weaknesses before choosing which one to use. This section will be devoted to the handling of Nek5000, and can serve as a brief introduction to the code.

4.1 NEK5000 BASICS

Nek5000 is a turbulent flow solver developed mainly by Paul Fischer and has through the past 20 years had several contributors. It is an open-source code applicable to many different types of flow and it has been put a lot of effort into the parallelization of the code, guaranteeing optimal speedup. All the parallelization is accessed through subroutines and functions, enabling the user to make advanced functions without having to deal directly with the functions from the MPI library. With SEM as the numerical method applied it is possible to obtain very accurate results.

Nek5000 provides some basic tools for generation of mesh. For more complex geometries this tool cannot compare with more visualized-based softwares such as ICEM from ANSYS which exports mesh to several numerical solvers such as Fluent and Nastran. It is therefore very useful to have an automatic way of converting a mesh created in ICEM to the format required by Nek5000. The way the mesh is created in this thesis is visualized in Figure 4.1.

FIGURE 4.1: *Visualization of how the mesh is created. The elemental mesh is first generated using ICEM, the script mshconvert converts this to a .rea-file and finally the distribution of the GLL-nodes is done during the initialization in Nek5000*

So far Nek5000 has supported three automatic routines for generating curved edges; circles in 2-D geometries, spherical shell elements and a general 2nd degree interpolation. Further manipulation of the element edges is left to the user to define manually for each particular problem. One of the objectives of this thesis is to make Nek5000 more user-friendly and create automatic routines to handle complex geometry. Before the work regarding the mesh routines are further elaborated an overview of the file-structure will be presented.
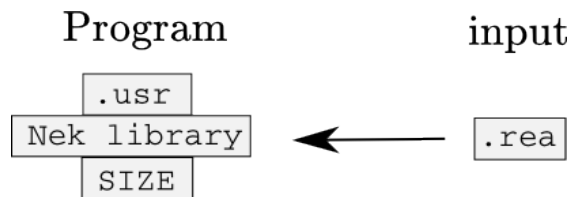
4.2 EDITABLE FILES

FIGURE 4.2: *Visualization of how the file structure in Nek5000 is built up.*

In order to work with Nek5000 there are some practical information that needs to be clarified. Nek5000 is recompiled for every case and the user specify all the case specific information in the three files {.rea,.usr,SIZE,}. .usr and SIZE are compiled with

the standard Nek5000 library using makenek which creates the executable file `nek5000`, they can be considered the surface and the core of the entire program. The `.rea` file contains case-specific information read during the initialization of the compiled program. The user guide [24] contains a tutorial which explains the necessary steps on how to get started with Nek5000. The next chapters will try to give some understanding on how the user is able to make the changes necessary for each case. Figure 4.3 illustrates how the files work together.

4.2.1 SIZE

Since Nek5000 is mostly based on Fortran77 all memory allocations are done statically and must be specified explicitly before runtime. Most of the variables used to determine the memory usage are stated in `SIZE`. The size of the working arrays necessary to perform the calculations are mostly defined by the upper limits of elements, processors, scalars and of course the polynomial degree of the local Lagrange functions. These variables define the sizes of almost all the arrays used in the program so it is important to define these variables as accurately as possible in order to optimize memory usage. The `SIZE` file can be considered as the necessary base for Nek5000.

4.2.2 .REA

In `.rea` all the problem specific parameters are given. While the content in `SIZE` is an absolute necessity to even compile the program the `.rea` file contains variables that are not used until the initialization of the case. The structure of the file is given in Table 4.1. Of the 103 variables specified in the beginning of the file there are roughly 50 of them that are used. Note that apart from the mesh information the `.rea` file restricts itself to single variables and boolean flags while the `.usr` needs to be applied for more advanced implementations.

4.2.3 .USR

This file contains a series of standard routines open for modification by the user. In addition the user is free to specify new routines if needed. A description of these routines

Lines	Section Name	Specifications
103	PARAMETERS	All problem-specific variables
K	PASSIVE SCALAR DATA	Convective and diffusive constants for scalars
K	LOGICAL SWITCHES	Boolean variables defining the solution method
E	MESH DATA	All nodes and elements are specified here
E	CURVED SIDE DATA	All the curved sides are specified here
E	FLUID BC	BC type for all elements and their faces
E	THERMAL BC	Thermal BC type for all elements and their faces
K	PRESOLVE/RESTART	Filename(s) of an initialized solution
K	INITIAL CONDITIONS	possibilities to specify IC further
K	OUTPUT FIELD	information that will be written to file

TABLE 4.1: *An overview of the different sections in .rea. E represents a predefined number depending on your problem which scales roughly as the number of elements, while $K \approx 1 - 25$ are user defined numbers.*

are given in the Nek5000 User manual [24]. A list of those frequently used for this thesis are described below,

- `userbc` - Define the boundary conditions on the inflow-boundary.

- `uservp` - Define variable properties, impose the eddy viscosity when applying LES.

- `userchk` - Read inflow-data, and specify the output.

- `usrdat2` - Project the geometry onto a deformed general surface. The details of how this routine is used will be specified further in Chapter 5.

- `usrdat3` - Defines the interpolation algorithm that is applied to the inflow-data.

In addition to these routines all user-defined functions are specified in this file. The LES implementation in Nek5000 is based on several subroutines specified in addition to those stated above. A list of some of the variables and functions applied for the implementations in this thesis are stated in Appendix B. The `.usr` file can be considered as the surface of Nek5000, easily accessible for the user.

4.3 THE BASICS OF THE SOLVER

The most important building blocks in Nek5000 are the `fluid` and `heat` functions which solves the N-S and Passive scalar equations. The N-S solver works very distinctly depending on the mathematical formulation enabled whereas the PS equation, which does

not depend on the pressure, is solved similarly for $P_N P_N$ and $P_N P_{N-2}$. For the sake of clarity, Figure 4.3 shows how the algorithms are called from the main routine. This is a very simplified flow chart which does not include choices such as filters, preconditioners, LES-model, de-aliasing etc. but it explains how the two main algorithms are selected using the boolean variable `ifsplit`.
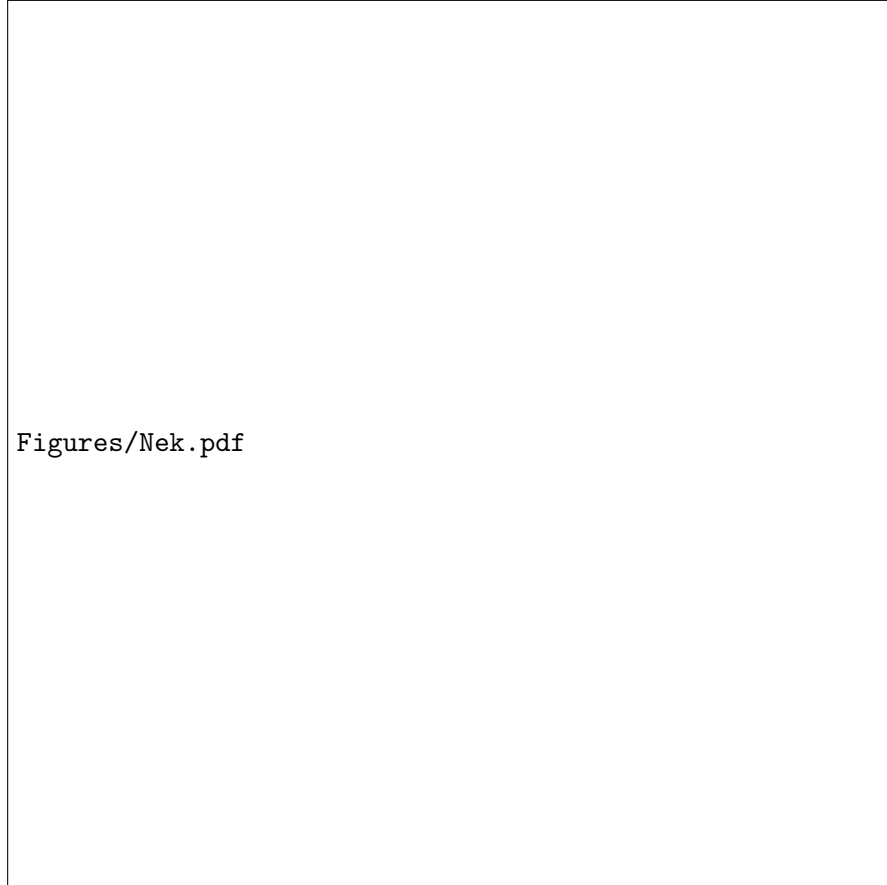
Figures/Nek.pdf

FIGURE 4.3: *Visualization of the steps in Nek5000.*

The description of the routines corresponding to Pressure-correction and fractional step are found in Chapter 3.5.4 and 3.5.3. For further details regarding the implementation in Nek5000 it is referred to [26] and [31]. As mentioned before an important difference between these two implementations is the fact that the $P_N P_N$ implementation is based on an analytical splitting algorithm which introduces a non-vanishing error in the pressure along the boundaries of the domain while the $P_N P_{N-2}$ algorithm is a discrete splitting which does not explicitly force a wrong boundary condition. It is however argumented in for instance [23] that the discrete splitting also introduces an erroneous boundary condition weakly.

4.4 Nek5000 for complex geometries

For complex curved geometries such as bent cylinders, spheres, ellipsoids etc. the user has to be able to express these surfaces analytically and write a routine in `usrdat2` that projects the points of interest onto the surface. Even for a simple shape such as a sphere some implementation has to be done and it demands that the user has knowledge to Fortran77 and the structure of Nek5000.

The necessary implementation consists of two steps

1. determine the faces that belong to the deformed surface

2. project the predefined GLL-points onto the deformed surface

This can be done without too much work for shapes with a known analytical expression such as a cylinder or a sphere, but for some general CAD geometry it is no way to perform this projection routine. This is a vulnerable point for a SEM solver since the elements generated by the mesh are relatively coarse. Many Finite volume based solvers do not support curved elements simply because the complex geometries are resolved with a sufficiently high resolution and it is of no interest to approximate them any better. However for a spectral element solver it is necessary to address this problem since spectral convergence for the approximated solution in $\mathbb{P}_N$ is not achievable if the geometry is only represented in $\mathbb{P}_1$ or $\mathbb{P}_2$.

As a part of this thesis two advancements have been made regarding complex geometries. The first part is a fully automatic procedure which projects any edge onto a circle. This is a convenient method when working with cylinder geometries and other similar shapes. The second part is an attempt to include general boundary surfaces by creating a semi-automatic procedure allowing the user to represent any geometry with polynomials of the same order as applied for the basis functions. The algorithms are presented in Chapter 5.

CHAPTER 5

IMPLEMENTATION

This chapter aims to present the implementations done in this thesis. The routines implemented are meant to develop Nek5000 functionalities in the encounter with complex geometries.

As shown in Figure 4.1 the coarse element grid is created in ICEM and then converted using the python script `mshconvert` while the distribution of GLL-nodes and the simulation itself was performed in Nek5000. This procedure has its limitations regarding the distribution of the GLL-nodes. This is due to the fact that `.rea` only contains information about the corners and the edges of the elements.

5.1 PROJECT EDGES ONTO A SPECIFIED ARC

The Gordon Hall (GH) algorithm that is described in Chapter 3.4.4 was already implemented as a function in the Nek library. By defining the GLL-nodes on the curved edges such that they correspond to an arc, the GH-algorithm is able to distribute the internal nodes accordingly.

The curved edges are specified in `.rea` and have until now been read as a second degree polynomial or as a part of a spherical shell. The routine `xyzarc()` was created to process curved edges specified in `.rea` with a radius and center. It can be considered as an alternative to the already implemented `xyzquad()` in `genxyz.f` which generates curved edges represented as second order polynomials. The algorithm is described below and Figure 5.1 gives a visual representation of the situation.

The two end nodes of the edge are denoted a, b, c is the mid node of the edge, θ is the full angle of the circle sector, cc is the center coordinates, g denotes the vector containing the GLL-points in $[-1, 1]$ and r will be the radius.

```
l = a-b                        ! vector between the corner nodes
c = (a+b)/2                     ! midpoint location
h = c-cc                        ! height of the framed triangle
θ = arctan(abs(l)/2*abs(h))     ! half the angle of the circle sector
g = g*θ                         ! angles to the GLL-points on the circle-sector
!---------- Finding the intersecting points ----------!
!---- x on the line l, and extend x-cc to the arc ----!
do k=1,lx1          ! for the number of nodes in one direction
    α = h*tan(g[k])            ! offset from the midpoint on l
    x = c-α*l/abs(l)           ! actual coordinate on l
    m = x-cc                   ! hypotenuse of the imposed triangle
    edge(k) = cc+r*m/abs(m)    ! final coordinate on the arc
enddo
```

This code defines the GLL-nodes on a circle sector corresponding to the radius and circle center provided in section `CURVED SIDE DATA` in `.rea`. The remaining operation is to call the Gordon Hall algorithm and create the internal GLL-points. To make
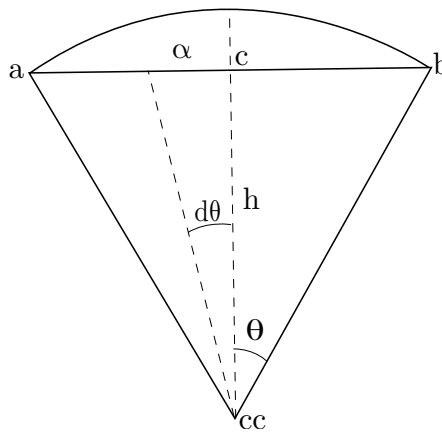

FIGURE 5.1: *A sketch of the curved edge and the variables necessary to calculate the projection*

this implementation fully automatic a small change in the script `mshconvert` was also necessary. Since ICEM provides the midpoints of the curved edges, a function was added to convert the midpoint information originally provided to a circle center and its correspoding radius.

add this procedure to the appendix?? along with averaging and other routines?

5.2 General surface projection

The routine `xyzarc()` enables the user to more accurately represent circular edges. For more complex geometry such as actual terrain and other surfaces without any analytic expression the large element sizes make the geometrical representation difficult. Theoretically the GLL-points can be projected onto a non-analytical surface, but since the element mesh is created in a different program the necessary information is not available to Nek5000. The idea is to create an additional fine surface mesh in ICEM such that the nodes in this mesh describes the surface fine enough to distribute the GLL-nodes correctly in Nek5000. During the initialization of the mesh in Nek5000 the program can read this information and project the GLL-nodes onto the provided surface. The routine was made as automatic as possible, and can be summarized in these four steps

1. Create initial Mesh and convert to `.rea` applying mshconvert.

2. Create refined surface mesh on the non-regular surface.

3. Enable projection by setting param(33) = 1.

4. Choose number of interpolation points by modifying param(34)= (1,2,3)

In addition to the standard Nek library the file `surfpro.f` needs to be added to the folder `trunk/nek/` along with all the other scripts applied by Nek5000. This implementation could be done directly in `.usr`, but it is of practical interest to keep this file as tidy as possible. Two external files are also generated by the modified mshconvert script for the algorithm to work. `surf.i` contains all the coordinates to the points on the refined surface. `bdry.i` contains the element, and face number to all the faces to be projected onto the surface.

The algorithm is best explained through a simple box with a non-regular floor. An example of this situation is the hill of Ekeberg. Before describing the algorithm let $E_{tot} = n_x n_y n_z$ be the total number of elements, N is the polynomial degree and let us for simplicity assume that $n_x = n_y = n_z$ such that $E = E_{tot}^{2/3}$ is the number of elements containing a face on the non-regular surface. The number of points on the refined surface N_s should be approximately EN^4 in order to describe the surface for all the GLL-points that belong to the boundary. This estimate assumes that the surface mesh

is equidistantly distributed whereas the GLL-nodes are denser along the boundaries of each element, $\Delta x_{min} = \mathcal{O}(1/N^2)$.

The pseudo code for the algorithm is listed below with the temporal costs commented out.

```
do e,f in bdry.i    !O(E)
  wrk = create_working_surface(e,f)  !O(EN^4)
  do i in GLL-nodes   !O(N^2)
    interp = init_interpolation_array() !O(1)
    do j in wrk    !O(N^4)
       update_int_array(interp,wrk(j)) ! O(1)
    enddo
    set_new_point(interp,wrk,i,e,f) ! O(1)
  enddo
  fix_GLL() !O(N^3)
enddo
fix_geom()
```

In order to understand the algorithm a short description of the auxiliary functions is given in the list below

- create_working_surface(e,f) – Loops through all the nodes in surf.i and adds the surface-coordinates within a certain radius to the center of face f on element e to the array wrk. This saves time in the search for interpolation points for each GLL-node.

- init_interpolation_array() – initializing the array containing the closest points on the surface for the current GLL-node.

- update_int_array(interp,wrk(j)) – compares the current surface point to the already existing interpolation points and adds it to the list if it is found to be closer to the initial GLL-node.

- set_new_point(interp,wrk,i,e,f) – updating the new GLL-point determined by the surface points in interp.

- fix_GLL() – There is a risk after distributing the GLL-points on the surface that some of the internal GLL-points falls outside the element. This function distributes all internal GLL-points correctly between the newly projected face and the opposite.

- fix_geom() – An already existing Nek routine that redistributes the GLL-points to assure that the distance between them on the new surface is correct.

Although this routine is only called once, and therefore will not contribute significantly to the total runtime of the program it is desirable to have a fast algorithm. Another analysis important to be made is the amount of extra storage space needed for this algorithm. By analysing the pseudo code the time of the algorithm should be of order $\mathcal{O}(E(EN^4 + N^2N^4 + N^3)) = \mathcal{O}(EN^4(E + N^2))$ and the amount of additional storage space will be of order $\mathcal{O}(EN^4 + E + N^2) = \mathcal{O}(EN^4)$.

The routine attempts to be as automatic as possible and the only implementation necessary is a call from `usrdat2` with 3 input variables.

Now an illustrative example of how this method is applied by the user. Say you have a project called "myFlow", and the mesh and surface mesh created in ICEM are named mesh_myFlow and surfmesh_myFlow. The following commands are then executed

```
>> /nmshconvert --mesh mesh_myFlow
    --reafile init.rea --outfile myFlow.rea
    --tol 1e-3 --temperature True --curvetype A

>> ./nmshconvert --mesh surfmesh_myFlow
    --mesh_format surface
```

After running the commands above the only thing left is to change parameters 13 and 14 in `.rea` and add `call surfpro()` to `usrdat2`.

5.2.1 TEST OF THE PROJECTION ROUTINE

To test the algorithm described in Chapter 5.2 the hill of Ekeberg in Oslo and a helicopter body was used. These surfaces were loaded as `.tin` files in ICEM and coarse hex meshes were created around the surfaces. The domains are presented in given in Figure 5.2, notice the coarse element sizes in the figure to the right. These geometries were chosen because they resemble a typical problem with spectral elements. Since the initial element-mesh is relatively coarse it does not capture all the details in the geometry and the GLL-nodes distributed on the faces corresponding to the unstructured surface will
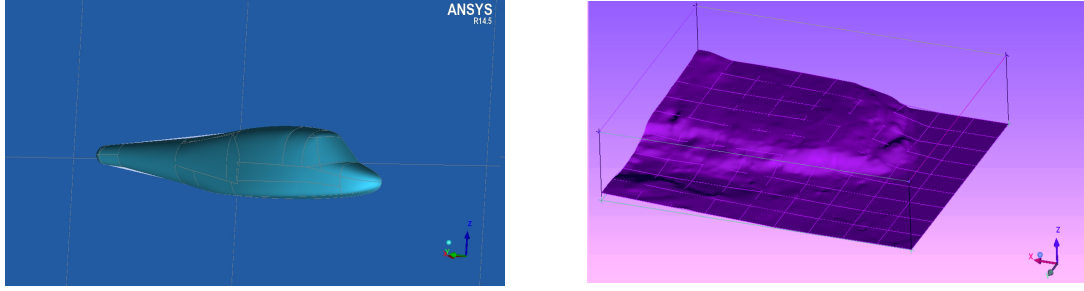
FIGURE 5.2: *Two examples of smooth surfaces with no analytical expression. To the left is the body of a helicopter, to the right is the hill of Ekeberg.*

be misplaced. With the routine described in Chapter 5.2 the surface is approximated accurately by higher order polynomials. The algorithm restricts itself to relatively smooth surfaces, since the polynomial describing the surface is typically of order $N \approx 7$.

5.3 SPATIAL AVERAGING ROUTINE

A dynamic Smagorinsky model has previously been implemented in Nek5000 for flow in a channel. The SGS-model as described in Chapter 2 depends on an averaging routine to calculate the dynamic Smagorinsky constant. The previous implementation in Nek5000 applies an average routine in the plane, assuming that the Smagorinsky constant is the same for all points with equal distance to the walls of the channel. This is a rather case specific averaging routine based on the assumption of homogeneous turbulence in the entire plane, hence only applicable to flows in idealized geometries.

When applying dynamical Smagorinsky to Case 1 a new spatial mean routine had to be applied for it to be stable. It was first attempted to average only in time, but this proved not to be sufficient. It was therefore implemented a routine for taking the average within each element, let c_{num}^e, c_{den}^e denote the numerator and the denominator in Eq. (2.26). The means are then calculated as

$$c_{num}^e = \frac{1}{V} \int_{\Omega_e} c_{num}^e d\,\Omega \approx \frac{1}{V} \sum_{i=1}^{N^3} \rho_{i,e} c_{num,i}^e. \qquad (5.1)$$

And similarly for c_{den}^e. The coefficients $\rho_{i,e}$ are found in the array `BM1(lx1,ly1,lz1)` in the file `MASS`.

CHAPTER 6

CASE STUDIES AND RESULTS

This chapter will present the cases investigated and the results achieved. The main tools in addition to Nek5000 needed to perform the simulations presented in this chapter are *ANSYS ICEM* and *python*. For post-processing *Visit* and *Matlab* were used.

6.1   CASE 1: GAS DISPERSION IN A SIMPLIFIED URBAN AREA

The scenario investigated in this work is dispersion of a neutral gas in a rectangular tunnel with four cubic blocks placed as obstacles. The blocks have sides $h = 0.109$m and represent a set of buildings forming a street canyon. The gas is released from a circular source on ground level and is translated by the wind field through the canyon, see Figure 6.1. In this figure h have been used as the length scale. The dotted lines indicate the positions where data is collected.

Scaling the domain with the size of the boundary layer $H = 1$m restricts it to the box $0.0 \leq x/H \leq 4.96, -1.75 \leq y/H \leq 1.75, 0 \leq z/H \leq 1.5$. The four cubic boxes are centered around $(1.4315, 0)$ with a distance h between each box. The source is placed with its center in $(0.396, 0)$ and radius $r = 0.0515$. The grid used for the computations consists of 14747 elements and with a polynomial degree of 8 the total number of nodes $N \approx 7, 6$mill.

The simulations are performed using Large Eddy Simulation (LES) with the dynamic Smagorinsky-Lilly subgrid-scale model and by applying the polynomial filtering routine
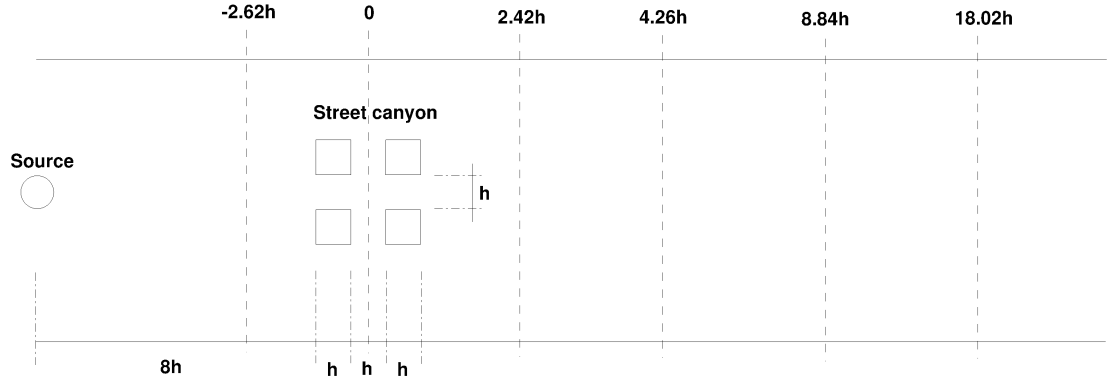
FIGURE 6.1: *Schematic overview of the domain from above. The data is collected along the dotted lines.*

Variable	value	unit	commentary
H	1	m	length scale of the domain
h	0.109	m	the sides of the cubic boxes
Q	50	dm^3/min	gas release from source
U_{ref}	≈ 1.08	m/s	reference value of U

TABLE 6.1: *Essential variables, U_{ref} is calculated as a time average of the velocity in x-direction at a point far away from the floor and walls and will therefore vary by a small amount from case to case.*

that is available in Nek5000. The release of gas will result in a plume that is advected with the wind field, see Figure 6.3. The concentration of the released gas at the indicated positions in Figure 6.1 are compared with experimental data and simulations performed in CDP [32]. For clarification some of the variables repeatedly mentioned throughout this thesis will be stated explicitly in Table 6.1.

The inflow conditions had to be extrapolated onto the domain at each time step. To mimic the situation in the wind-tunnel the velocity field on the inflow was generated in a different simulation performed in CDP. The inflow velocity was written to file every 0.0013s for a total of 28s and had to be interpolated onto the domain for the simulations in Nek5000 since the grid was not identical. The right plot in Figure 6.2 is an instantaneous picture of the inflow velocity in x-direction, notice how the pattern repeats itself along the y-axis. This is because the inflow data was generated in a smaller channel, $\approx 1/3$ of the width of the computational domain used for the data sampling. An interpolation algorithm implemented at FFI was applied in order to adjust the inflow-data to the computational mesh, this was done directly in `.usr`.
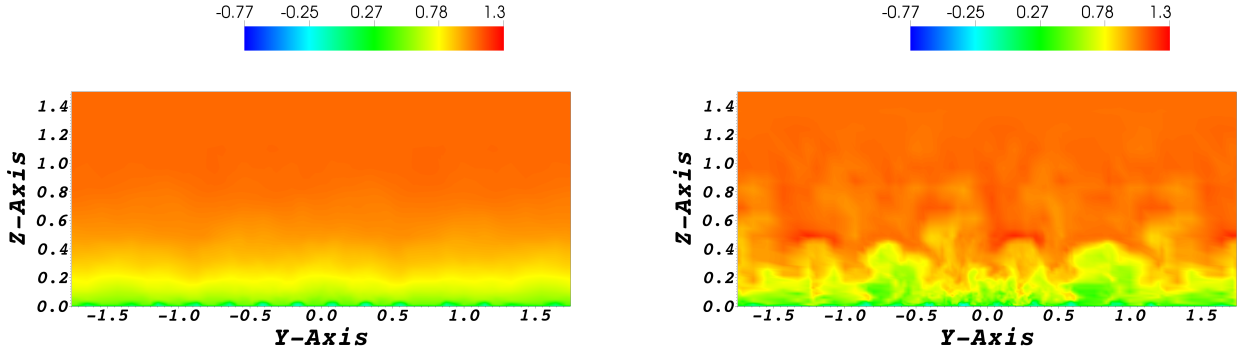
FIGURE 6.2: *The averaged (left) and instantaneous (right) x-velocity on the inflow boundary.*

The simulations in Nek5000 were performed in the following manner; first 6 seconds of initialization of the velocity field in the channel, followed by 8 seconds of gas release to initialize the gas-concentration. After assuring that the wind-field was correctly created and the released gas had reached the measurement lines furthest from the source the data sampling of 22 seconds started.
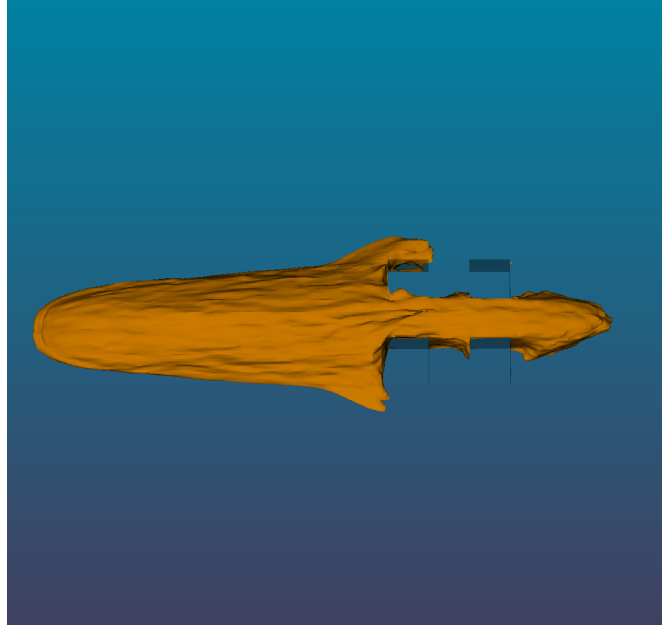

FIGURE 6.3: *An iso-surface of the average concentration with $C = 0.03$ after 30 seconds of sampling.*

6.1.1 RESULTS - GAS DISPERSION

This case is a part of a larger project designed to evaluate different solvers ability to perform simulations of gas dispersion. The N-S equations are solved using the $P_N P_N$ formulation with the fractional step method, IOFS with a target Courant number equal 2 was enabled to maximize the time step as recommended in [24]. It should be mentioned that the stability properties when activating the SGS-model and deactivating the filtering was greatly reduced. This effect is captured in Figure 6.4 that shows how the Smagorinsky model does not damp spurious velocity modes in the same degree as the filter.
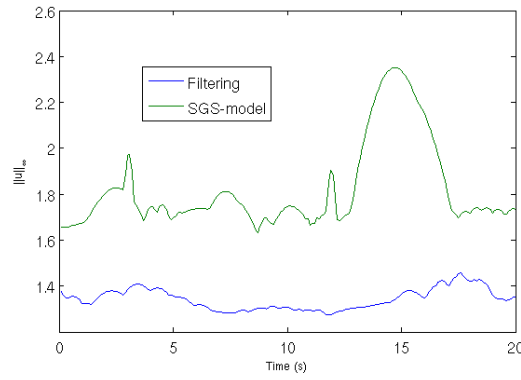

FIGURE 6.4: $||\mathbf{u}||_\infty$ *as a function of time, the green line represents the simulation with the dynamic Smagorinsky SGS-model and the blue line represents the filtering with* $\alpha = 0.05$ *and a quadratic decay on the last 3 modes.*
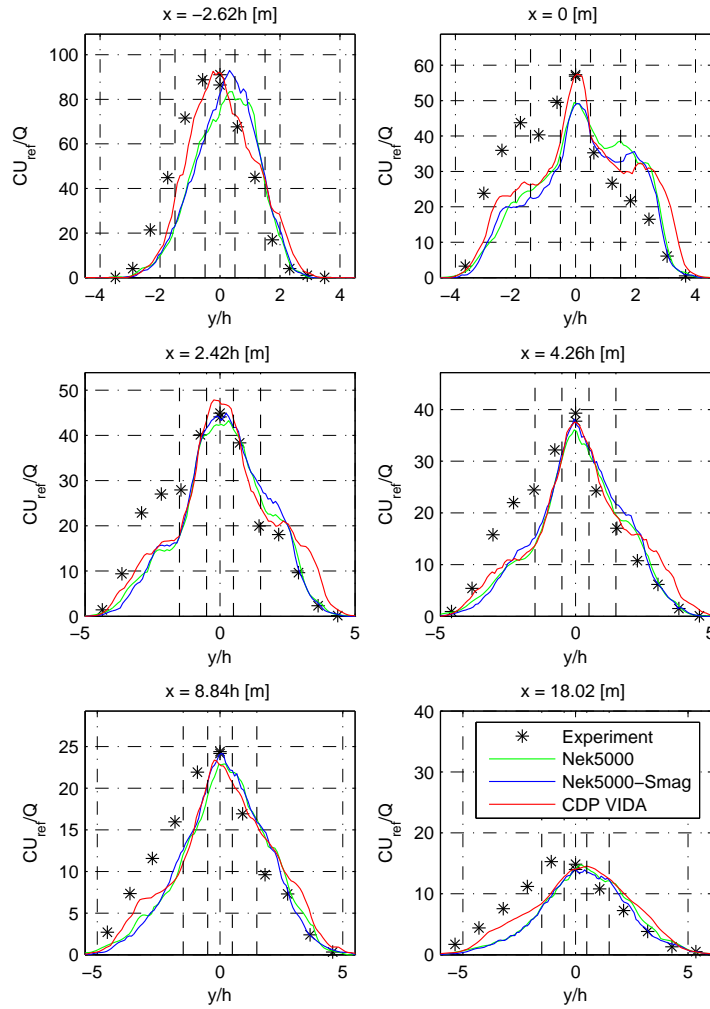
FIGURE 6.5: *Time-averaged concentration with a sample time of* 22.00 *s at* $y = 0$ *plotted vertically and scaled with the free-stream velocity and emission rate. Compared against wind tunnel data. Two dashed lines on either side of the centerline represent the canyon.*

Figure 6.5 shows the scaled concentration along the dotted lines in Figure 6.1. According to this figure Nek5000 does indeed capture the important features of the mean concentration. At the two first measurement lines the results are slightly skewed to the right, this is to some degree also the case for the CDP simulations but not for the experiment. A possible explanation could be that the inflow condition favours one of the sides of the domain, or simply that the sampling time is not sufficiently long.

The results also indicate that the difference between the SGS-model and filtering is not that large, if anything the SGS-model shows a tendency to estimate lower concentration

peaks. This could be a result of too much smoothing due to the turbulent viscosity. An important difference between the filtering and the SGS-model is the fact that the filter works based on the current state of the flow whereas the amount of diffusion added by the SGS-model is mostly decided by the previous states of the flow. This could lead to either too much or too little smoothening locally.
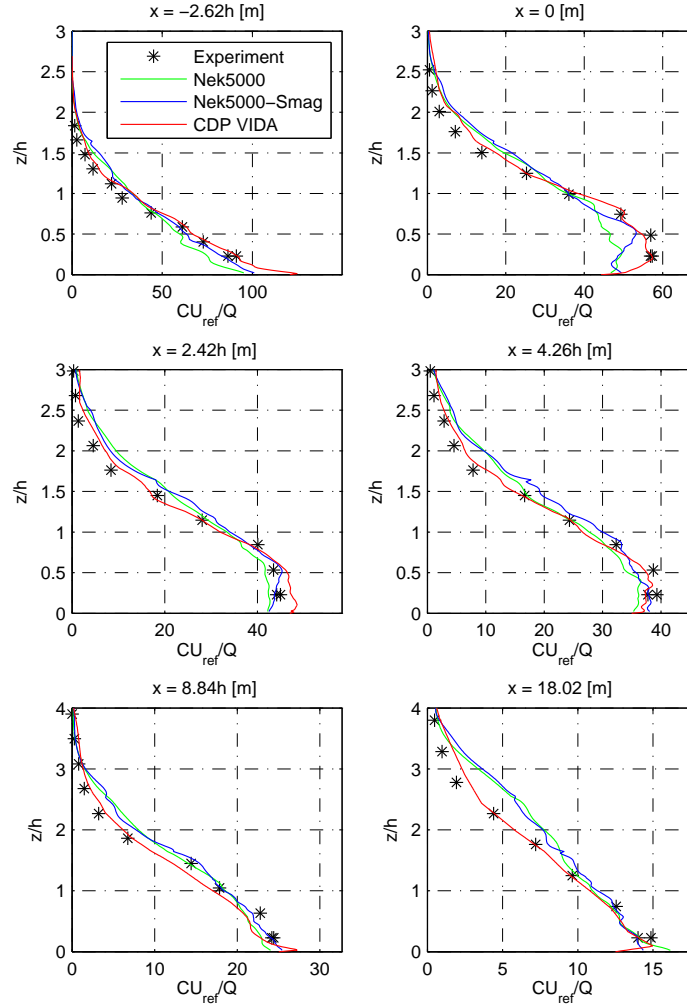
FIGURE 6.6: *Time-averaged concentration with a sample time of* 22.00 *s at* $y = 0$ *plotted vertically and scaled with the free-stream velocity and emission rate. Compared against wind tunnel data. Two dashed lines on either side of the centerline represent the canyon.*

The concentration along the vertical measurement lines is plotted in Figure 6.6 and overall Nek5000 provides good results according to the reference solutions. The largest difference is found close to the wall right in the middle of the cubes. In particular the simulation including the SGS-model underestimates the concentration in this domain. It is known that the Dynamic Smagorinsky model does not perform that well close to the wall which could be a partial explanation to this. Along with the fact that the $P_N P_N$ spitting errors also could be significant close to the wall.

6.2 Case 2: Drag and lift on a cylinder

A standard benchmark case for flow solvers is presented in [33]. The case is to calculate the drag and lift coefficients on a cylinder in a rectangular channel. The setup for the domain and boundary conditions are given in Figure 6.7. The constants applied in the description of the geometry and the coefficient scales are listed in table Table 6.2. Finding the drag and lift coefficient requires a calculation of the velocity field around

Constant	Value	Property
H	0.41m	Width and height for the channel
D	0.1m	Diameter of the cylinder and length scale
U	0.2m/s	Velocity scale
ν	$10^{-3}\text{m}^2/\text{s}$	Kinematic viscosity of the fluid
Re	20	Reynolds number

TABLE 6.2: *Constants for case 2*

the cylinder which is done by solving the unsteady N-S equations until a steady flow is reached. This implies that the spatial accuracy will dominate the error and one would expect great results in Nek5000 due to its spectral convergence rate.

The flow is laminar with Reynolds number $Re = 20$ so all the challenges arising when dealing with turbulent flow does not come to play in this case. The drag and lift forces
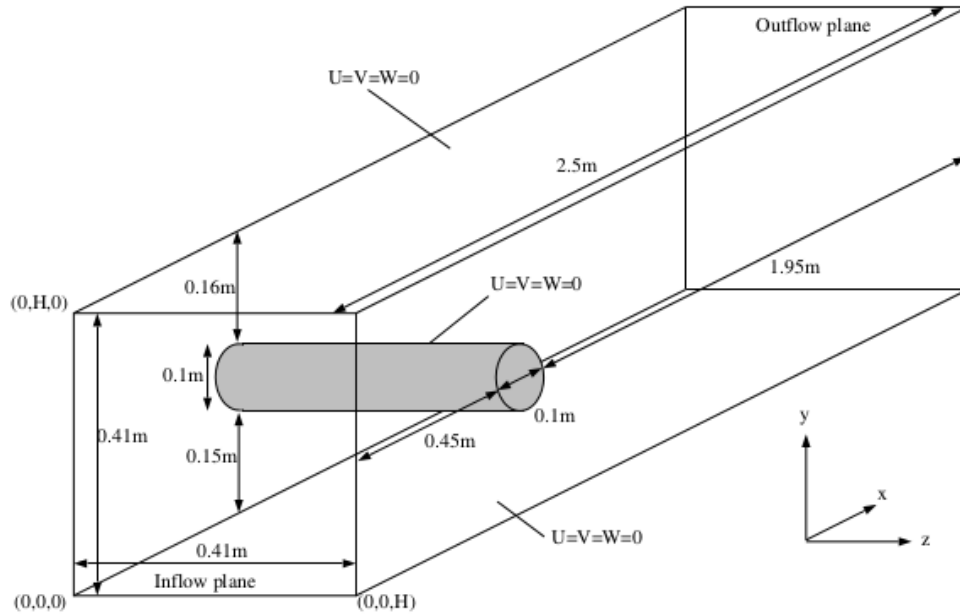

FIGURE 6.7: *Computational domain and boundary conditions.*

on a surface S are given as

$$F_D = \int_S (\rho\nu\frac{\partial v_t}{\partial n}n_y - pn_x)dS, \qquad F_L = -\int_S (\rho\nu\frac{\partial v_t}{\partial n}n_x + pn_y)dS. \qquad (6.1)$$

v_t is the tangential velocity, $\mathbf{n} = [n_x, n_y, 0]$ is the unit vector normal to the surface S and the tangent velocity vector is defined as $\mathbf{t} = [n_y, -n_x, 0]$.

Surface integrals in Nek5000 are solved numerically, $\int_S f dS = \sum f_i A_i$, where f is some function and A_i is the area corresponding to the nodal value f_i. A_i corresponds to a two dimensional mass matrix in Nek5000 available for all elements.

The coefficients corresponding to these forces known as the drag and lift coefficients are given by the formulas

$$c_D = \frac{2F_D}{\rho U^2 DH} \qquad , \qquad c_L = \frac{2F_L}{\rho U^2 DH}. \qquad (6.2)$$

Nek5000 provides functions for calculating lift and drag on any user-specified object. The function is called `drag_calc(scale)`, with the input parameter defined by the user, for this case `scale` $= 2/(\rho U^2 DH)$. Apart from this the function `set_obj()` has to be modified in order to create an object that consists of pointers to all the faces on the cylinder. The mesh around the cylinder is illustrated in Figure 6.8. Initially this case was
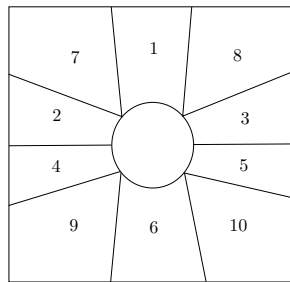

FIGURE 6.8: *Initial mesh around cylinder.*

solved using a second degree polynomial to describe the circle segments corresponding to each element. However with the new routine implemented as described in Chapter 5.1 the circle segments could be represented with the same order as the polynomials used

for the velocity space. The importance of the error resulting from the second degree approximation of the circle segments is presented in Chapter 6.

An additional test that is performed on this case is how different settings in Nek5000 will affect the estimation of the drag and lift coefficients. Perhaps most curious is whether the $P_N P_N$ or $P_N P_{N-2}$ formulation is applied. Note that the pressure in the latter formulation is not defined on the boundary of the cylinder and does therefore need to be extrapolated onto the surface in order for the integral to be calculated. On the other side is the splitting scheme implied by the $P_N P_N$ forces the erroneous boundary condition on the pressure.

6.2.1 Results - benchmark comparison

The effect of the algorithm explained in Chapter 5.1 is illustrated by solving a laminar flow test problem. The solution is compared with previously benchmark computations performed by a number of contributors [33].

The results are presented in Table 6.3, and they confirm that the treatment of the geometry is essential, both coefficients are computed with significantly better accuracy. Compared with the results from the other softwares applied in [33] Nek5000 performs

# of Cells	Software	c_D	c_L	%**Err** c_D	%**Err** c_L
2755170	Nek5000 (mid)	6.18349	0.008939	0.030	4.19
2755170	Nek5000 (arc)	6.18498	0.009413	0.006	0.13
3145728	CFX	6.18287	0.009387	0.04	0.15
3145728	OF	6.18931	0.00973	0.06	3.5
3145728	FEATFLOW	6.18465	0.009397	0.01	0.05

TABLE 6.3: *Results for the drag and lift coefficients with reference values $c_D = 6.18533$ and $c_L = 0.009401$. $p = 11$ for the simulations in Nek5000.*

just as well or better in most cases. It should be mentioned that the division of the grid is created in a different manner for Nek5000 so the comparison is not as direct as it may seem from the table.

6.2.2 Results - internal adjustments

As discussed in Chapter 4 there are many adjustments available in Nek5000. In order to enlighten the actual effect on the results, several different settings were investigated

for this case and the results are presented in Table 6.4. The spectral convergence is also confirmed in Figure 6.9 by calculating the lift coefficient error for increasing polynomial degree.
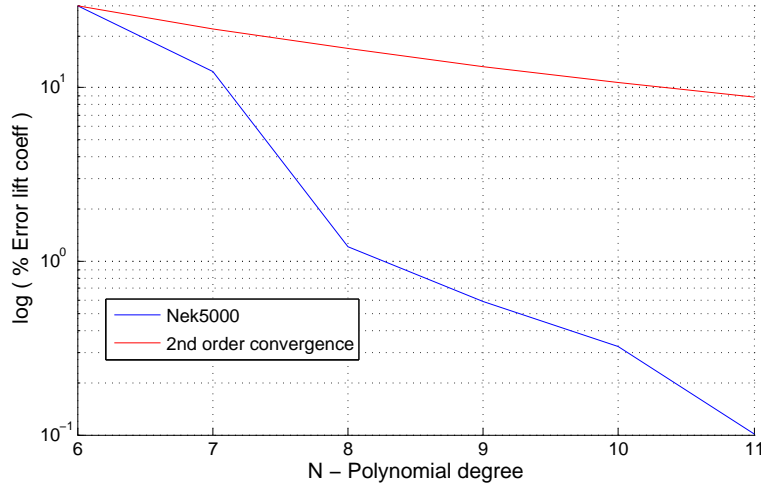

FIGURE 6.9: *The logarithm of the error plotted against the polynomial degree. All results are with $P_N P_{N-2}$ and dealiasing, and they are solved without using the characteristic scheme or any filtering. A line illustrating a second order convergence is plotted to illustrate the convergence rate.*

The setting that has the biggest impact on the result is the $P_N P_N$ scheme which clearly performs worse than the others. This is as expected since the discrete splitting is known to converge faster for steady state flows. Notice however that by reducing the time-step the effect of the algebraic splitting greatly reduces and achieves results of similar order as the discrete splitting. Use of the IOFS method also has a negative effect on the accuracy, this is also as expected because of the stability-accuracy trade-off for this method. Remember that this scheme allows a much higher time step. The filtering is the least significant change which confirms the analytical results from Eq. (3.32).

		Settings				% Error	
#	Δt	ifsplit	Dealiasing	IOFS	Filter	c_D	c_L
1	8e-3	No	Yes	No	No	0.005	0.10
2	8e-3	Yes	Yes	No	No	0.013	2.35
3	8e-3	No	Yes	No	Yes	0.005	0.43
4	8e-3	No	Yes	Yes	No	0.005	0.18
5	8e-3	No	No	No	No	0.005	0.03
6	4e-3	Yes	Yes	No	No	0.004	0.49

TABLE 6.4: *Test of solver settings in Nek5000.*

Be aware that these results are obtained from a laminar test case and does not in any way suggest any optimal adjustment for Nek5000. An important example of this is the fact that deactivating de-aliasing yields better results. For a coarser mesh or a more turbulent flow this would not be the case, and that the result is actually better is probably due to the accuracy, which are very close to the accuracy given by the reference solution. The resuslts do however give an indication to the general effect of these settings that are worth noticing.

6.3 DISCUSSION AND CONCLUSION

How did Nek5000 perform overall, user-friendly ?,correctness,speed etc.

Appendix A

Fundamental basics of

numerical analysis

A.1 Legendre polynomials

The Legendre polynomials are a group of orthogonal polynomials on $(-1, 1)$ satisfying the recurrence relation

$$(k + 1)L_{k+1}(x) = (2k + 1)xL_k(x) - kL_{k-1}(x), \tag{A.1}$$

where $L_0(x) = 1$ and $L_1(x) = x$. Some other useful properties are the L_2-norm and the derivatives which can be found in any texbook, for instance [12],

$$||L_k(x)||^2 = \int_{-1}^{1} L_k(x)dx = \frac{2}{2k + 1},$$
$$L'_{k+1}(x) = (2k + 1)L_k(x) + L'_{k-1}(x). \tag{A.2}$$

By continuing the recursive form of the second line in Eq. (A.2) one obtains

$$L'_{k-1}(x) = (2(k - 2) + 1)L_{k-2}(x) + L'_{k-3}(x),$$
$$L'_{k-3}(x) = (2(k - 4) + 1)L_{k-4}(x) + L'_{k-5}(x), \tag{A.3}$$
$$\vdots$$

Which ultimately enables an expression for the derivative based on the lower order Legendre polynomials, explicitly given as

$$
\begin{aligned}
L'_{k+1}(x) = {}& (2k+1)L_k(x) \\
& + (2(k-2)+1)L_{k-2}(x) \\
& + (2(k-4)+1)L_{k-4}(x) + \cdots
\end{aligned}
\tag{A.4}
$$

Notice that the coefficients in front of each polynomial is 2 times the inverse norm of the same polynomial squared, allowing the expression to be simplified to

$$
\begin{aligned}
L'_{k+1}(x) = {}& 2||L_k||^{-2}L_k(x) \\
& + 2||L_{k-2}||^{-2}L_{k-2}(x) \\
& + 2||L_{k-4}||^{-2}L_{k-4}(x) + \cdots
\end{aligned}
\tag{A.5}
$$

In this thesis the second order derivatives will be used and by the result in Eq. (A.6) they will be given as

$$
\begin{aligned}
L''_{k+1}(x) = {}& 2||L_k||^{-2}L'_k(x) \\
& + 2||L_{k-2}||^{-2}L'_{k-2}(x) \\
& + 2||L_{k-4}||^{-2}L'_{k-4}(x) + \cdots
\end{aligned}
\tag{A.6}
$$

Applying the same recurrence relations from Eq. (A.6) to the rhs. derivatives and assembling the terms allows the second derivative of the Legendre polynomial to be written as

$$
\begin{aligned}
\frac{1}{4}L''_{n+1}(x) = {}& ||L_n||^{-2}||L_{n-1}||^{-2}L_{n-1}(x) \\
& + \left(||L_n||^{-2} + ||L_{n-2}||^{-2}\right)||L_{n-3}||^{-2}L_{n-3}(x) \\
& + \left(||L_n||^{-2} + ||L_{n-2}||^{-2} + ||L_{n-4}||^{-2}\right)||L_{n-5}||^{-2}L_{n-5}(x)\cdots
\end{aligned}
\tag{A.7}
$$

This can be written in a compact form as

$$
L''_{n+1}(x) = \sum_{j=1}^{\lceil n/2 \rceil} \Lambda_{n+1,n+1-2j}L_{n+1-2j}(x),
\tag{A.8}
$$

$$
\Lambda_{n+1,n+1-2j} = 4||L_{n+1-2j}||^{-2}\sum_{k=0}^{j+1}||L_{n-2k}||^{-2}.
\tag{A.9}
$$

The sum $\Lambda_{i,j}$ can be considered as the coefficient describing the amount of L_i'' which is described by L_j. For the sake of clarity Λ is restated here with indices i, j

$$\Lambda_{i,j} = 4||L_j||^{-2} \sum_{k=1}^{(i-j)/2+1} ||L_{i+1-2k}||^{-2}. \tag{A.10}$$

Appendix B

Variables and Functions in Nek5000

B.1 Variables

The Nek manual provides information on many of the variables given in the .rea and SIZE file. It is however no list of useful variables defined in other files. Below is a list of some of the variables that have been frequently used in .usr subroutines which initially are defined outside of both SIZE, .rea and .usr.

B.2 Functions

B.2.1 standard calculations found in math.f or navier1.f

nekasgn(ix,iy,iz,ie) Assigns the coordinates of node (ix,iy,iz) in element ie to the common variables x,y,z

facind(kx1,kx2,ky1,ky2,kz1,kz2,nx1,ny1,nz1,f) Assigns the index limits of a face f with nx1,ny1,nz1 points in each spatial direction.

zwgll(zg,wg,nx1) Get the nx1 GLL-points and weights to zg and wg.

cadd(zg,c,nx1) Adding a constant c to a vector zg of length nx1.

AVG

uavg(ax1,ay1,az1,lelt)	Averaged values of u, similar for v,w,p
urms(ax1,ay1,az1,lelt)	Variance of u, similar for v,w,p
vwms(ax1,ay1,az1,lelt)	Covariance of vw
tavg(ax1,ay1,az1,lelt,ldimt)	Averaged values of t and all passive scalars

GEOM

xm1(lx1,ly1,lz1,lelt)	X-coordinates for the velocity mesh
xm2(lx2,ly2,lz2,lelv)	X-coordinates for the pressure mesh
unx(lx1,lz1,6,lelt)	Surface normals

INPUT

cbc(6,lelt,0:ldimt1)	Boundary conditions of each face
ccurve(12,lelt)	Curved side character
curve(12,6,lelt)	Curved side information

PARALLEL

lglel(lelt)	Mapping from local to global element index
gllel(lelg)	Mapping from global to local element index

SOLN

vx(lx1,ly1,lz1,lelv)	X-velocity
t(lx1,ly1,lz1,lelv,ldimt)	Temperature and passive scalars
vtrans(lx1,ly1,lz1,lelt,ldimt1)	Diffusive constant to additional scalars
vdiff(lx1,ly1,lz1,lelt,ldimt1)	Convective constants to additional scalars

TSTEP

istep	Current iteration step
iostep	Output step frecuency
time	Current time
tstep	Current timestep
dt	Timestep
dtlag(10)	The preevious 10 timesteps
bd(10)	Max 10 backward difference coeffs
ab(10)	Max 10 extrapolation coeffs (Adam-Bashforth)

WZ

zgm1(lx1,3)	GLL points for x,y and z directions

WZF

zgl(lx1)	Gauss lobatto points
wgl(lx1)	Gauss lobatto weights

OTHER

x,y,z	Local coordinates assigned by nekasgn()
ux,uy,uz	Local velocities assigned by nekasgn()
temp	Local temperature assigned by nekasgn()
nio	Processor node number
ndim	Number of dimensions
nelv	Number of elements for velocity mesh
nelt	Number of elements for the t-mesh
pm1 (lx1,ly1,lz1,lelv)	Pressure mapped to mesh 1

TABLE B.1: *useful variables in Nek, the bold capital sections denote the seperate files in /trunk/nek/.*

cmult(zg,c,nx1) Multiplying every element of vector zg of length nx1 with c.

chsign(wrk,nx1) change the sign of every element in vector wrk of length nx1.

cfill(zg,c,nx1) Fill vector zg of lenght nx1 with the constant c.

rzero(zg,nx1) Fill vector zg of length nx1 with zeroes.

rcopy(zg,zg2,nx1) copy all elements from vector zg2 to vector zg, both of lenght nx1.

B.2.2 Functions regarding mesh and distribution of GLL-points

gh_face_extend(x,zg,n,type,e,v) The Gordon hall algorithm described in chapter 3, the type variable denotes whether the algorithm should use vertices, edges or faces to distribute the inner GLL-points.

xyzlin(xl,yl,zl,nxl,nxl,nxl,e,ifaxl) Generate bi- or trilinear mesh.

fix_geom() Routine for re distributing the gll-points corrctly on the updated geometry.

B.2.3 Additional auxiliary functions implemented for this thesis

fix_gll(e,f) Redistribute the gll-points between the given face and the opposite to make sure that all points lie within the element.

getface(kx1,kx2,ky1,ky2,kz1,kz2,wrk,n,e) assigning the values of the face in element e corresponding to the index limits kx1,kx2...to the array wrk of size n*n*3.

getsurfnorm(sn,ix,iy,iz,f,ie) Providing the surface normal sn at point ix,iy,iz of element ie and face f

calcerror(error,lambda,sn,wrk,radius) calculate the distance from the initial gll-point to a given point on the surface.

interp_up(iinterp,rinterp,error,k) Update interpolation points

set_new_pt(iinterp,rinterp,ix,iy,iz,e) defining the position of the new gll-point on the surface

getlimits(k,n,kx1,kx2,ky1,ky2,kz1,kz2) Get the index limits kx1,kx2... corresponding to edge k with n gll-points.

setcoords(xq,yq,zq,xedge,yedge,zedge,nxl,k) copy the updated edges xedge to the initial edges xq

getcoords(xq,yq,zq,xedge,yedge,zedge,nxl,k) copy the node information from the initial edge xq to xedge

Bibliography

[1] F. M. White. *Viscous fluid flow.* McGraw-Hill series in mechanical engineering. McGraw-Hill, New York, 1991. ISBN 0-07-069712-4. URL http://opac.inria.fr/record=b1096847.

[2] D. Carati, G. S. Winckelmans, and H. Jeanmart. On the modelling of the subgrid-scale and filtered-scale stress tensors in large-eddy simulation. *Journal of Fluid Mechanics*, 441:119–138, 8 2001. ISSN 1469-7645. doi: 10.1017/S0022112001004773. URL http://journals.cambridge.org/article_S0022112001004773.

[3] A. Leonard. Energy cascade in large eddy simulations of turbulent fluid flows. *Adv. Geophys.*, 18A:237–248, 1974.

[4] S. B. Pope. *Turbulent Flows.* Cambridge University Press, 2000. ISBN 9780511840531. URL http://dx.doi.org/10.1017/CBO9780511840531. Cambridge Books Online.

[5] D. K. Lilly. The representation of small scale turbulence in numerical simulation experiments. In *IBM Scientific Computing Symposium on environmental sciences*, pages 195–210, Yorktown heights, 1967.

[6] M. Germano, U. Piomelli, P. Moin, and W. H. Cabot. A dynamic subgrid-scale eddy viscosity model. *Phys. Fluids A*, 3:1760–1765, 1991.

[7] G. Karniadakis and S. Sherwin. *Spectral/hp element methods for computational fluid dynamics.* Oxford University Press, 2013.

[8] A. Quarteroni. *Numerical Models for Differential Problems, 2. edition.* Springer, 2014.

[9] I. Babuska. The finite element method with lagrangian multipliers. *Numerische Mathematik*, 20:179–192, 1972/73. URL http://eudml.org/doc/132183.

[10] F. Brezzi. On the existence, uniqueness and approximation of saddle-point problems arising from lagrangian multipliers. *ESAIM: Mathematical Modelling and Numerical Analysis - Modélisation Mathématique et Analyse Numérique*, 8(R2):129–151, 1974. URL http://eudml.org/doc/193255.

[11] J. L. Guermond. Nonstandard nonconforming approximation of the stokes problem, i: Periodic boundary conditions.

[12] C. Canuto, M. Y. Hussaini, and A. Quarteroni et al.i. *Spectral methods : evolution to complex geometries and applications to fluid dynamics*. Scientific computation. Springer, Berlin, 2007. ISBN 978-3-540-30727-3. URL http://opac.inria.fr/record=b1127560.

[13] E. Süli and D. F. Mayers. *An Introduction to Numerical Analysis*. Cambridge, 2006.

[14] Y. Maday and A. T. Patera. Spectral element methods for the incompressible navier-stokes equations. In *IN: State-of-the-art surveys on computational mechanics (A90-47176 21-64). New York, American Society of Mechanical Engineers, 1989, p. 71-143. Research supported by DARPA.*, volume 1, pages 71–143, 1989.

[15] A. T. Patera. A spectral element method for fluid dynamics: Laminar flow in a channel expansion. *Journal of Computational Physics*, 54(3):468–488, Jun 1984. ISSN 0021-9991. doi: 10.1016/0021-9991(84)90128-1. URL http://dx.doi.org/10.1016/0021-9991(84)90128-1.

[16] K. Z. Korczak and A. T. Patera. An isoparametric spectral element method for solution of the Navier-Stokes equations in complex geometry. *Journal of Computational Physics*, 62(2):361–382, Feb 1986. ISSN 0021-9991. doi: 10.1016/0021-9991(86)90134-8. URL http://dx.doi.org/10.1016/0021-9991(86)90134-8.

[17] Y. Maday, A. T. Patera, E. M. Ronquist, and Langley Research Center. *A well-posed optimal spectral element approximation for the Stokes problem*. National Aeronautics and Space Administration, Langley Research Center, 1987.

[18] P. F. Fischer and J. Mullen. Filter-based stabilization of spectral element methods. *Comptes Rendus de l'Académie des Sciences - Series I - Mathematics*, 332(3):265 – 270, 2001. ISSN 0764-4442. doi: http://dx.doi.org/10.

1016/S0764-4442(00)01763-8. URL http://www.sciencedirect.com/science/article/pii/S0764444200017638.

[19] R. Pasquetti and C.J. Xu. Comments on "filter-based stabilization of spectral element methods". *Journal of Computational Physics*, 182(2):646 – 650, 2002. ISSN 0021-9991. doi: http://dx.doi.org/10.1006/jcph.2002.7178. URL http://www.sciencedirect.com/science/article/pii/S0021999102971780.

[20] N. Young. *An Introduction to Hilbert Space.* Cambridge mathematical textbooks. Cambridge University Press, 1988. ISBN 9780521337175. URL https://books.google.no/books?id=_igwFHKwcyYC.

[21] T. J. R. Hughes, L. Mazzei, and K. E. Jansen. Large eddy simulation and the variational multiscale method. *Computing and Visualization in Science*, 3(1-2):47–59, 2000. ISSN 1432-9360. doi: 10.1007/s007910050051. URL http://dx.doi.org/10.1007/s007910050051.

[22] M. O. Deville, P. F. Fischer, and E. H. Mund. High-order methods for incompressible fluid flow. 2002. doi: 10.1017/cbo9780511546792. URL http://dx.doi.org/10.1017/CBO9780511546792.

[23] J. L. Guermond, P. Minev, and Jie Shen. An overview of projection methods for incompressible flows. *Computer Methods in Applied Mechanics and Engineering*, 195(44–47):6011 – 6045, 2006. ISSN 0045-7825. doi: http://dx.doi.org/10.1016/j.cma.2005.10.010. URL http://www.sciencedirect.com/science/article/pii/S0045782505004640.

[24] *NEK5000 documentation*, 2015.

[25] Y. Maday, A. T. Patera, and E. M. Rønquist. An operator-integration-factor splitting method for time-dependent problems: Application to incompressible fluid flow. *Journal of Scientific Computing*, 5(4):263–292, 1990. ISSN 0885-7474. doi: 10.1007/BF01063118. URL http://dx.doi.org/10.1007/BF01063118.

[26] P. F. Fischer and J. W. Lottes. Hybrid Schwarz-multigrid methods for the spectral element method. *J. Sci. Comput*, pages 45–78.

[27] J. B. Perot. An analysis of the fractional step method. *Journal of Computational Physics*, 108(1):51 – 58, 1993. ISSN 0021-9991. doi: http://dx.doi.org/10.

1006/jcph.1993.1162. URL http://www.sciencedirect.com/science/article/pii/S0021999183711629.

[28] S. Abdallah. Comments on the fractional step method. *Journal of Computational Physics*, 117(1):179 – 180, 1995. ISSN 0021-9991. doi: http://dx.doi.org/10.1006/jcph.1995.1055. URL http://www.sciencedirect.com/science/article/pii/S0021999185710558.

[29] J. B. Perot. Comments on the fractional step method. *Journal of Computational Physics*, 121(1):190 – 191, 1995. ISSN 0021-9991. doi: http://dx.doi.org/10.1006/jcph.1995.1189. URL http://www.sciencedirect.com/science/article/pii/S0021999185711898.

[30] J. van Kan. A second-order-accurate pressure-correction scheme for viscous incompressible flow. 7(3):870–891, 1986. ISSN 0196-5204. doi: http://dx.doi.org/10.1137/0907059.

[31] A. G. Tomboulides, J. C. Y. Lee, and S. A. Orszag. Numerical simulation of low mach number reactive flows. *J. Sci. Comput.*, 12(2):139–167, June 1997. ISSN 0885-7474. doi: 10.1023/A:1025669715376. URL http://dx.doi.org/10.1023/A:1025669715376.

[32] *CDP User's/Reference Manual v.2.4 - Stanford University.*

[33] S. Turek and M. Schäfer. Recent benchmark computations of laminar flow around a cylinder, 1996.